Single Solid Source Precursor Route to the Synthesis of MOCVD Cu-Cd-S Thin Films

B. Olofinjana[1*], A.C. Adebisi[1], F.O. Efe[1], O. Fasakin[1, 2], K.O. Oyedotun[2], M.A. Eleruja[1], E.O.B. Ajayi[1] and Ncholu Manyala[2].

[1]Department of Physics and Engineering Physics, Obafemi Awolowo University, Ile-Ife, 220005, Nigeria

[2] Department of Physics, Institute of Applied Materials, SARChI Chair in Carbon Technology and Materials, University of Pretoria, Pretoria 0002, South Africa.

*Corresponding Author, Tel: +234 8066762570, Email: olofinb@oauife.edu.ng

Abstract

Bis-(morpholinodithiato-s,s')-Cu-Cd was synthesized from appropriate reagents as a single solid source precursor and characterized using particle induced X-ray emission (PIXE), Fourier transform infrared (FTIR) spectroscopy and differential thermal analysis (DTA). Cu-Cd-S thin films were deposited on sodalime glass substrate using MOCVD technique at temperatures in the range 360 - 450 ^{o}C. The films were further characterized using Rutherford backscattering spectroscopy (RBS), X-ray diffraction (XRD), scanning electron microscopy (SEM), UV-visible spectroscopy and four-point probe technique. PIXE revealed that the synthesized precursor contained the expected elements which led to the successful deposition of the Cu-Cd-S thin films. FTIR ascertained that the organic ligand actually attached to the metals. DTA analysis showed that the synthesized precursor was thermally stable and could pyrolyzed around 300 and 500 ^{o}C. RBS of the deposited films showed that the stoichiometry and the thickness depended on deposition temperature. XRD analysis revealed that the films deposited at 360 and 380 ^{o}C are amorphous while those deposited at 400 to 450 ^{o}C showed peaks, which supported the possible co-existence of CuS and CdS as Cu-Cd-S, with an improvement in the crystallinity as substrate temperature increased. SEM showed that the films are uniform and crack-free, in which the morphology

strongly depended on substrate temperature. Optical analysis revealed that the films have high absorbance in the UV region and high transmittance in the visible and near infrared region, in which direct band gap energy of 2.36 to 2.14 eV was obtained as deposition temperature increased. Other optical parameters such as Urbach energy, refractive index, extinction coefficient, dielectric constant also increased as the deposition temperature increased. Electrical analysis showed that resistivity is temperature dependent as it reduced as deposition temperature increased.

Keywords: Single solid source precursor; Cu-Cd-S thin films; Band gap; Refractive index; Dielectric constant; Resistivity.

1. Introduction

Synthesis and characterization of metal chalcogenides have attracted the attention of researchers in recent years. This is due to their fascinating properties that can be of benefit for various applications such as diodes, photodetectors, sensors, thermistors, varistors, transistors, photovoltaics and solar cells, among others [1-7]. In such applications, high quality epitaxial films with appropriate structure and morphology are mostly desirable, since such can affect device performance. As a result, their structural, morphological, electrical, optical and magnetic properties have been widely studied either theoretically or experimentally.

Both cadmium sulphide (CdS) and copper sulphide are interesting metal chalcogenide with wide range of applications. CdS is an n-type semiconductor material which has been widely used as window material in heterojunction thin film solar cell devices because of its wide energy gap (2.42 eV) [8,9]. CdS is also an interesting material in the area of printed electronics, semiconductor lasers, light emitting diodes, transistors, nonlinear optical devices, etc., [10-14]. On the other hand, copper sulphide is a p-type semiconductor with different phases and stoichiometric forms, i.e. chalcocite (Cu_2S), djurlite ($Cu_{1.96}S$), digenite ($Cu_{1.8}S$), anilite ($Cu_{1.75}S$), covellite (CuS), and so on. Copper sulphide has wide range applications, which depend on the stoichiometry and the phase formed after synthesis. Different phases of copper sulphide have also received attention for their applications in solar cells, supercapacitors, sensors, lithium rechargeable batteries, among others, [15-19].

It has been proven that ternary and quaternary metal chalcogenides have more versatility, stability and efficiency in device fabrication than binary metal chalcogenides [20, 21]. Such versatility is based on the possibility that their physical and chemical properties can be tuned by simply varying the stoichiometry of their constituent elements. Furthermore, in order to overcome

some inherent defects in some binary chalcogenides, ternary and quaternary chalcogenides have been explored [21, 22].

Although both Cu_xS and CdS have similar crystal structure [23], their physical properties are quite different. Alloying both Cu_xS and CdS can provide varieties of unique physical properties to elevate the device applications of the individual Cu_xS and CdS counter-parts. Cu-Cd-S belongs to I-II-VI compound semiconductor materials having tunable properties between its Cu_xS and CdS counter-parts. Various synthesis techniques have been employed to synthesize Cu-Cd-S thin films. These include colloidal method, chemical bath, mechanochemical route, and spray pyrolysis [21, 24-26] among others. Among the various deposition techniques available, metal organic chemical vapor deposition (MOCVD) is a simple and inexpensive technique, which can yield good quality films and suitable is for large scale production. Generally, it requires no high-quality target and substrate; and our simple system does not require the use of vacuum at any stage. The use of single solid source also provides specific advantages such as simplifying the control of process parameters and avoiding the use of hazardous metal alkyls, H_2S and alkyl sulphide.

In this work, a single solid source precursor was synthesized from appropriate reagents. The precursor was characterized using particle induced X-ray emission (PIXE), Fourier transform infrared (FTIR) spectroscopy and differential thermal analysis (DTA). Thin films of Cu-Cd-S were deposited on sodalime glass substrate through the pyrolysis of the single solid source precursor using MOCVD technique at temperatures in the range 360-450 ^oC. The films were characterized using Rutherford backscattering spectroscopy (RBS), X-ray diffraction (XRD), scanning electron microscopy (SEM), UV-visible spectroscopy and four-point probe technique. To the best of our knowledge, this represents the first time of using a single solid source precursor for the deposition of Cu-Cd-S thin films.

2. Experimental

2.1 Precursor preparation and characterization

Preparation of the single solid source precursor, bis-(morpholinodithiato-s,s')-Cu-Cd, was done by modifying the procedure reported by Eleruja *et al*., [27]. Ammonium morpholino dithiocarbamate, which is the intermediate complex was prepared as follows: morpholine (8.7 cm^3, 0.1 mole) was added to ethanol (100 cm^3) while stirring and cooled to 0 ^oC in an ice-bath. Then, carbon disulfide (7.6 cm^3, 0.1 mole) was added drop-wise ensuring that the temperature of the solution did not rise above 5 ^oC. When the addition of carbon disulfide was completed, ammonia solution (75 cm^3) was immediately added to the reaction mixture to obtain a light-yellow solution. The resulting solution was put in a freezer for about 3 hours for crystallization and then filtered. The residue was left to air-dry, yielding ammonium morpholino dithiocarbamate (20.0 g, 86.6 % yield).

The prepared intermediate complex, ammonium morpholino-dithiocarbamate (17.31 g, 0.096 mole), was gradually dissolved in 1:1 of acetone-water solvent. Copper acetate (4.36 g, 0.024 mole) was dissolved in 3:1 of ethanol-water solvent while cadmium acetate (5.53 g, 0.024 mole) was also completely dissolved in 10 cm^3 of distilled water separately. The solutions of copper acetate in ethanol-water solvent and cadmium acetate in distilled water were added to the solution of ammonium morpholino-dithiocarbamate on a hot plate maintained at 60 ^oC and stirred vigorously. There was a spontaneous formation of brown precipitate as the addition continues. The precipitate formed was heated for about 30 minutes on the hot plate. The precipitate was then filtered and air-dried for about 24 hours, after which it was put in an oven maintained at a temperature of 60 ^oC to give 15.2 g (76% yield) of bis-(morpholinodithiato-s,s')-Cu-Cd.

Elemental composition of the single solid source precursor was determined using particle induced X-ray emission (PIXE) with a 3.0 MeV proton obtained from the ion beam analysis (IBA) facility at the Center for Energy Research and Development (CERD), Obafemi Awolowo University, Ile-Ife, Nigeria. The facility is a NEC 5SDH 1.7 MV Pelletron Tandem accelerator equipped with a RF charge exchange ion source, which provide proton and helium ions. A Canberra Si(Li) detector (model ESLX 30-150) was used for X-ray data acquisition. The PIXE spectrum was then analyzed using GUPIXWIN software.

Functional group identification in the synthesized single solid source precursor was done using Fourier transform infrared spectrophotometer - Shimadzu PYE-Unicam SP3-300 spectrophotometer. The precursor was grinded with KBr to a fine powder and pressed into a pellet. Background spectrum was obtained and converted to frequency data by inverse Fourier transform. The background spectrum was then subtracted from the sample spectrum to obtain the actual information about the sample. The spectrum of the sample was obtained from the ratio between single beam sample spectrum and the single beam background spectrum. Data analysis was done by assigning the observed absorption frequency bands in the precursor spectrum to appropriate normal modes of vibrations in the molecules.

Differential thermal analysis (DTA) was used to study the thermal property of the precursor. This was done using a NETZSCH 4040PC differential thermal analyzer at the Center for Energy Research and Development (CERD), Obafemi Awolowo University, Ile-Ife, Nigeria. 10 mg of the precursor was placed in the DTA cell and heated from 25 to 500 °C at a heating rate of 10 °C min^{-1}. The material (precursor) under study and an inert reference were made to undergo identical thermal cycles (i.e. same cooling or heating program) and the temperature difference between the

sample and reference were recorded. The heat flow (differential temperature) was then plotted against temperature.

2.2 Thin film deposition and characterization

The set-up for the deposition of Cu-Cd-S thin films is as shown in Figure 1. The precursor was grounded to a fine powder and placed in an unheated receptacle, and dried nitrogen gas was bubbled through at a flow rate of 2.5 dm^3/min. The nitrogen-borne particles were then transported into the working chamber, which consist of an electrically heated pyrex tube maintained at various deposition temperatures (360 - 450 ^oC). Inside the chamber, the substrate was supported on a stainless-steel block for good and uniform thermal contact. On reaching the hot zone, the precursor bis-(morpholinodithiato-s,s')-Cu-Cd first sublimed before thermal decomposition whereby thin films of Cu-Cd-S was deposited on the substrate surface. The typical decomposition time was 2 hours. The substrate used was sodalime glass slide with composition (at. pct) O, Si, Na, Ca, Mg, Al = 60, 25, 10, 3, 1, 1. The whole operation was carried out in a fume hood, so as to minimize some of the handling problems associated with metal organic compounds.

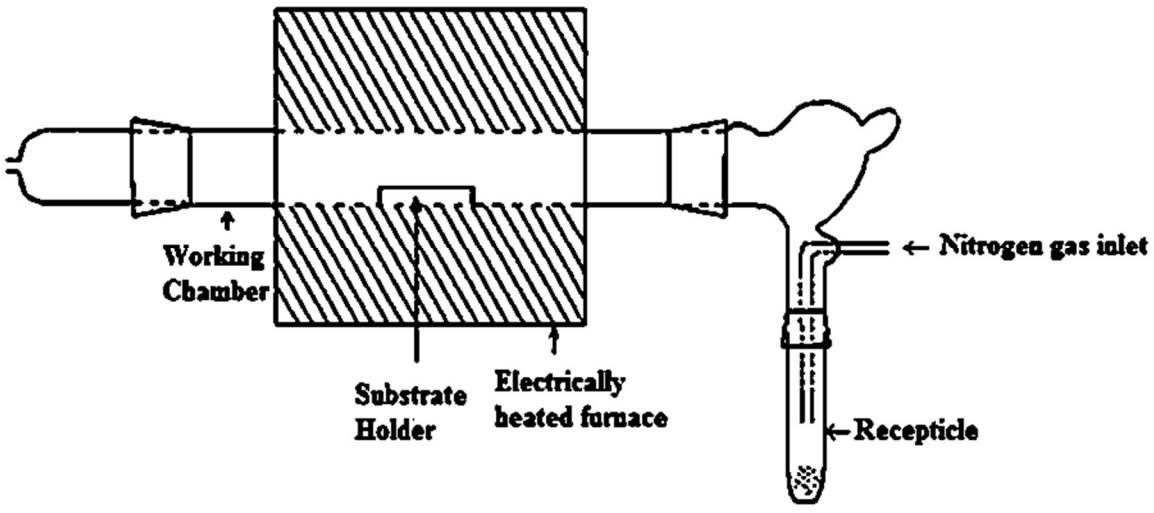

Figure 1: Set-up for the deposition of the thin films

The elemental composition, stoichiometry and thickness of the deposited Cu-Cd-S thin films were determined using Rutherford backscattering spectroscopy (RBS). The facility used for the PIXE of the precursor was also used for the RBS of the films. $^{4}He^{+}$ of energy 2.2 MeV and beam current of 3.8 nA with integrated beam dose of 10.0 μC was used as incident beam. The scattering configuration used was the IBM geometry with detector solid angle of 0.833 msr and a resolution of 12 KeV. The extracted RBS spectrum from the silicon detector of the IBA facility was then analyzed using SIMNRA fitting code.

X-ray diffraction of the as-deposited film was carried out using a Radicon X-Ray Mini-diffractometer (Model: MD-10). The diffractometer uses a high voltage source of 25 kV with radiation of CoKα line of wavelength 0.179 nm. The diffraction angle was in the range of 5 to 80°. Multiple data sets were collected, with each set covering slightly more than half a full rotation of the film. The intensity was then plotted against 2θ.

The morphology of the thin films was done using ultra plus 55 field emission scanning electron microscope (FESEM). The prepared samples were cut into dimension 1 cm x 1 cm and coated with gold (to avoid charging effect), which subsequently improve the micrograph. The electron beam, which has an energy ranging from 0.2 keV to 40 keV and nominal resolution of 1 nm, was focused by a condenser lens to a spot of about 0.4 nm to 5.0 nm in diameter. Secondary electrons were acquired and amplified to produce SEM micrograph images at different magnifications operated at an accelerated voltage of 10 kV.

Double beam PYE UNICAM SP8-400 UV-visible spectrophotometer was used to study the optical properties of the films. A beam of light from a source was separated into its component wavelengths by a prism or diffraction grating. Each monochromatic beam was in turn split into two equal intensity beams by a half-mirrored device. The ultraviolet (UV) region scanned was

from 200 to 400 nm, and the visible portion was from 400 to 800 nm. The spectrometer records all the wavelengths at which absorption occurs together with the amount of absorption at each wavelength. The instrument then creates a spectrum of absorbance versus wavelength.

Four-point collinear probe configuration technique was used for the electrical analysis of the deposited Cu-Cd-S thin films. A high impedance current source was used to supply current through the outer two probes while a voltmeter measures the voltage across the inner two probes. The current-voltage characteristic of the films was then determined. A Keithley 2400 source meter was used for the current-voltage measurements.

3. Results and discussions

3.1 PIXE of the prepared precursor

Figure 2 shows the PIXE spectrum of the prepared precursor bis-(morpholinodithiato-s,s')-Cu-Cd. The spectrum is a plot of counts against channels, which was generated by GUPIXWIN software. Prominent peaks in the spectrum are associated with sulphur, copper and cadmium in the prepared precursor. From Table 1, the concentration ratio of Cu to Cd is 0.63, which indicates that Cu to Cd ratio in the precursor is not in one to one correspondence. Therefore, the prepared bis-(morpholinodithiato-s,s')-Cu-Cd precursor consists of expected elements which can lead to the deposition of Cu-Cd-S thin films.

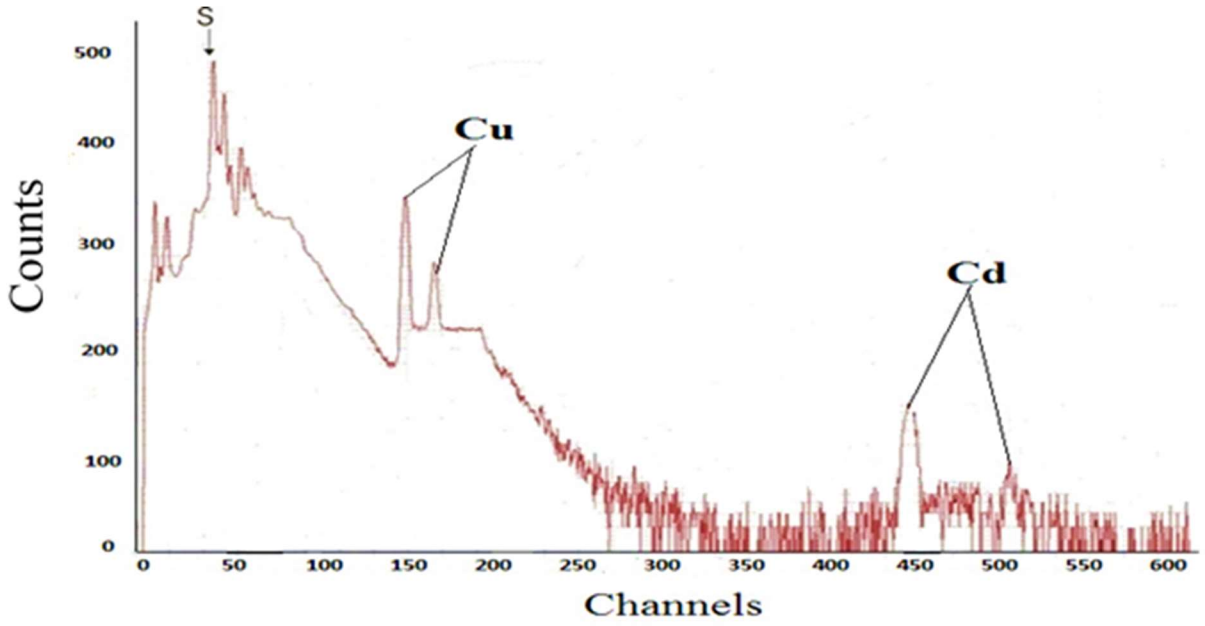

Figure 2: PIXE spectrum of bis-(morpholinodithiato-s,s')-Cu-Cd

Table 1: Elemental composition of bis-(morpholinodithiato-s,s')-Cu-Cd

Element	Concentration (ppm)
S	744484.6
Cu	150624.0
Cd	240534.6

3.2 FTIR of the prepared precursor

The IR spectrum of the precursor obtained in KBr shows that the precursor exhibits the basic absorption bands between 4000 cm^{-1} and 400 cm^{-1} (Figure 3). The observed major peaks are at 3421.83 cm^{-1}, which correspond to O-H stretching vibration of water molecules, C-H vibrations at 3122.86 and 2854.74 cm^{-1}, C=O stretching at 1984.82 and 1637.62 cm^{-1}, C-C stretching at nearly 1483.31 and 1232.55 cm^{-1}, δC-H at about 877.64 cm^{-1}, as well as C-S at around 655.82 cm^{-1}, respectively. All these are the characteristics bands of organic ligand, which ascertained that the ligand was really attached to the metals (Cu, Cd) and sulphur. Metal-sulphide bands, Cu-S and Cd-S are from 540.09 cm^{-1} and below.

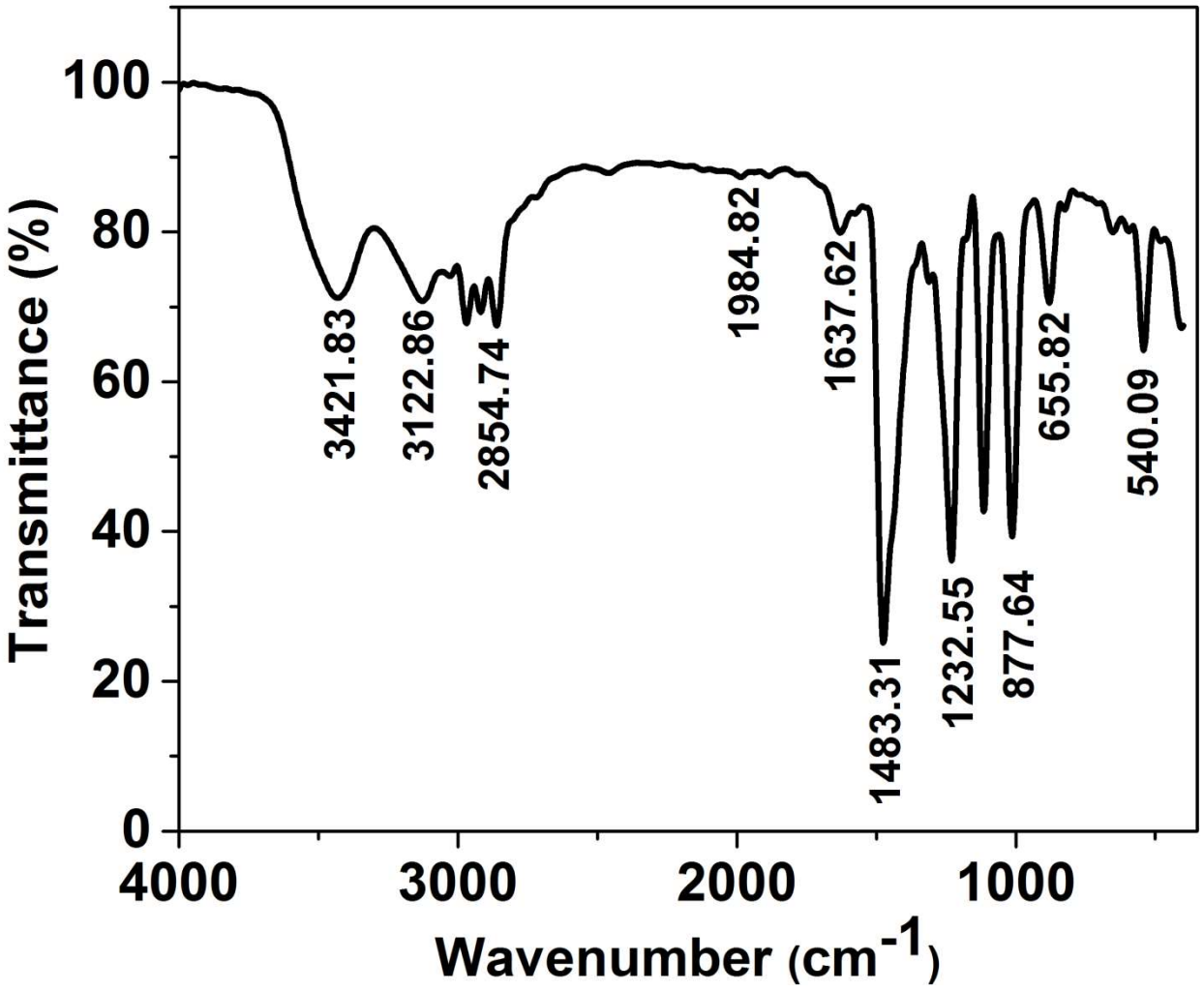

Figure 3: FTIR Spectrum of bis-(morpholinodithiato-s,s')-Cu-Cd

3.3 DTA of the prepared precursor

DTA of the precursor was done so as to ascertain the thermal behaviour of the precursor and to predict the range of temperature at which the precursor will pyrolyze. The spectrum in Figure 4 shows the DTA curve of the precursor. An exothermic peak was observed at a temperature of 247 ºC corresponding to a reduced weight of -3.411 mW/mg, which was caused by oxidative decomposition. The exothermic peak indicates heat evolved from the sample, since the temperature of the tested sample during the phase transformation/chemical reaction is higher than

the reference temperature. There was phase transition upon heating due to the hydroscopic nature of the precursor. From the thermograph, it can also be observed that the precursor may pyrolyze around 300 ºC and 500 ºC leading to the deposition of Cu-Cd-S thin films. Also, the precursor is thermally stable in air.

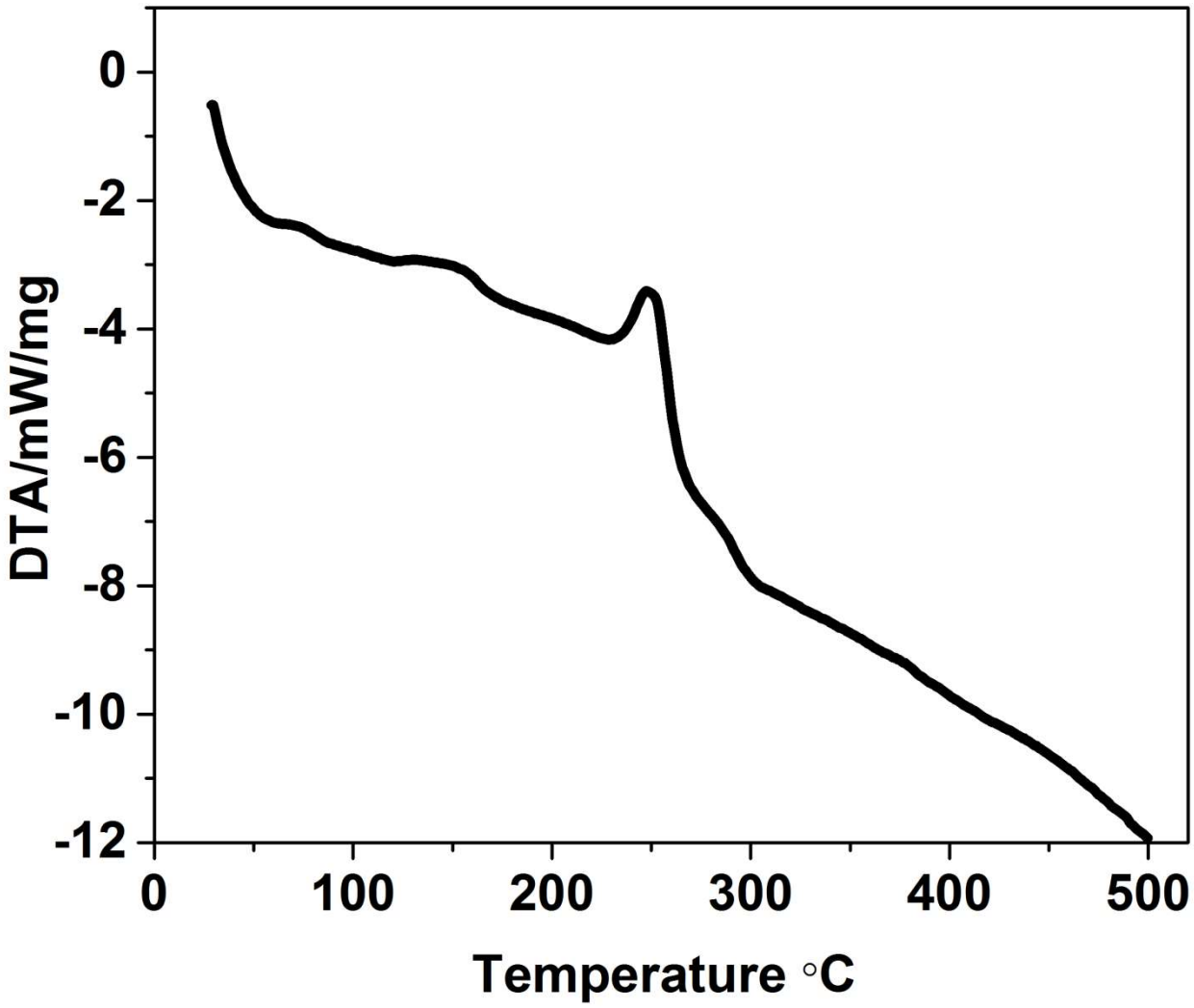

Figure 4: DTA thermograph of bis-(morpholinodithiato-s,s')-Cu-Cd

3.4 RBS analysis of Cu-Cd-S thin films

Rutherford backscattering spectroscopy (RBS) was used to determine the elemental composition and thickness of the films. A typical RBS spectrum of the films is shown in Figure 5. The RBS spectrum revealed the presence of Cu, Cd and S as the constituent elements of the

deposited films. Table 2 summarizes the compositional analysis and thickness of the films deposited at various deposition temperatures. From the compositional analysis of both the precursor and the deposited films, it was observed that the ratio of Cu to Cd in the precursor was not preserved in the deposited films. This can be attributed to breakdown of metal-metal bonds of the precursor in the vapor phase at different deposition temperature and subsequent gradual reconstitution of the bonds [27]. Similar result has been reported for during the deposition of $Zn_xCd_{1-x}S$ thin films [27]. From Table 2, it should be noted also that (Cu+Cd)/S ratio is not fixed, which implies that the deposited Cu-Cd-S thin films are non-stoichiometry. The abundance of sulphur in the films may be attributed to the starting material as there is higher concentration of sulphur in the precursor. The film thickness was observed to increase from 40 to 70 nm as the deposition temperature increases from 360 to 450 ^{o}C. This can be as a result of increase in the rate of nucleation in the hot zone as the deposition temperature increases. As the deposition temperature increases, more thermal energy is produced which then accelerates decomposition of the precursor by increasing the rate of chemical reaction in the working chamber. This is in accordance with what was reported in the literature [28].

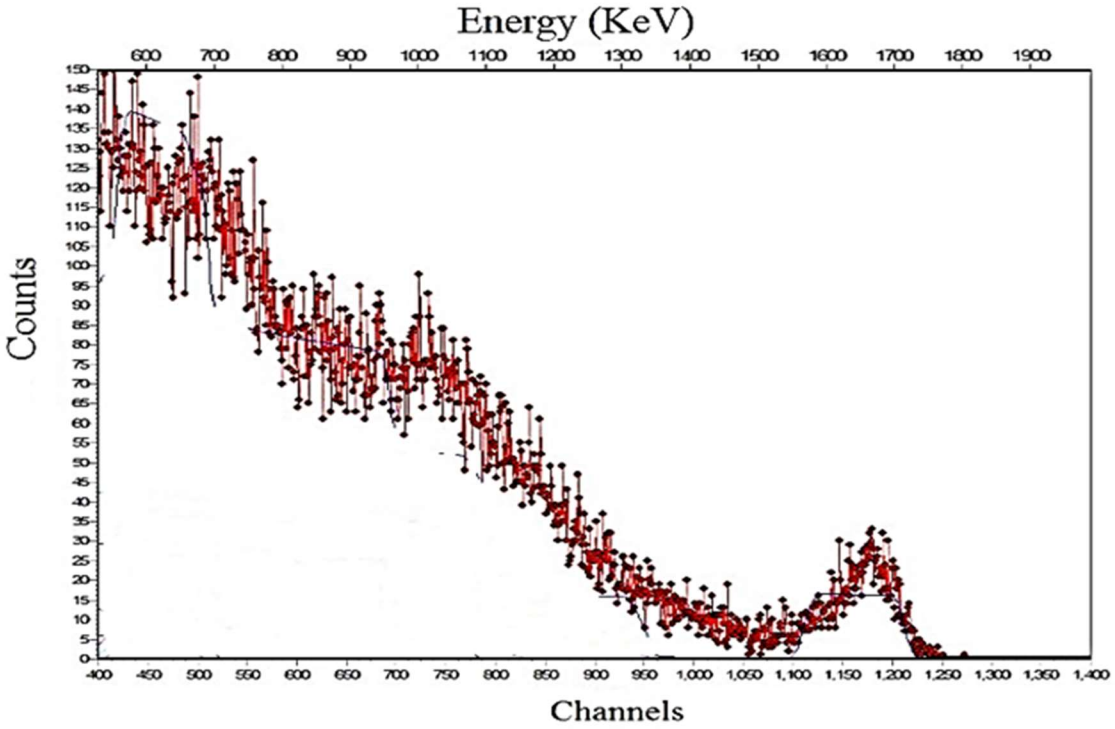

Figure 5: Typical RBS spectrum of the deposited Cu-Cd-S thin film

Table 2: Summary of the compositional analysis and thickness with respect to deposition temperature.

Deposition temperature (°C)	Composition (%)			(Cu+Zn)/S	Thickness (nm)
	Cu	**Cd**	**S**		
360	3.83	32.83	63.50	0.58	40
380	6.28	17.32	76.40	0.31	50
400	7.32	14.85	77.83	0.28	60
420	3.67	15.71	80.62	0.24	65
450	4.59	10.20	85.21	0.17	70

3.5 Structural analysis of the deposited Cu-Cd-S thin films

The structural analysis of the deposited films was done using XRD in the range of diffraction angle, 2θ from 5 to 80 °. The XRD spectrum is shown in Figure 6. The spectrum at 360 and 380 °C has no peak probably due to amorphous nature of the films deposited at those temperatures. Three peaks were observed at deposition temperature of 400 °C at 2θ values of

11.40°, 23.54°, 32.66°, corresponding to planes (101), (003), and (103). At 420 °C, peaks were observed at 2θ values of 12.07°, 20.15°, 30.95°, which corresponds to diffraction planes (101), (003), and (103). Film deposited at 450 °C has four peaks at 2θ values of 10.61°, 16.09 °, 30.91° and 37.61° which correspond to diffraction planes (101), (003), (103) and (102). There are no *JCPDS* data available for Cu-Cd-S phase [29, 30]. Hence the diffraction peaks from various (h k l) planes were compared to peaks of CuS (JCPDS: PDF #75-2233) and CdS (JCPDS: 02-0563) phases. The presence of (003), (103) and (102) normally occurs at the same 2θ values for CuS and CdS phase. This makes it difficult to actually identify the phase which those peaks correspond to between CuS and CdS. The planes (101) and (102) at 2θ values 10.61° and 37.61° corresponds to wutzite hexagonal of CdS (JCPDS: 02-0563). The close lattice arrangement between CuS and CdS supports the possible co-existence of CuS and CdS as Cu-Cd-S single phase [21, 23].

Observation from XRD patterns of the deposited films showed an improvement in the crystallinity of the films when substrate temperature was increased. This is from the fact that the number of peaks increase as the deposition temperature increases. Also, a slight shift of the diffraction peaks at 2θ value 23.54° towards a higher angle was observed at higher temperature. This might be due to surface restructuring caused by the incorporation of Cu in the crystal lattice of CdS. This implies that Cu^{+} can successfully be incorporated into the lattice of CdS, similar result has been reported by Kumar *et al*., 2018 [31].

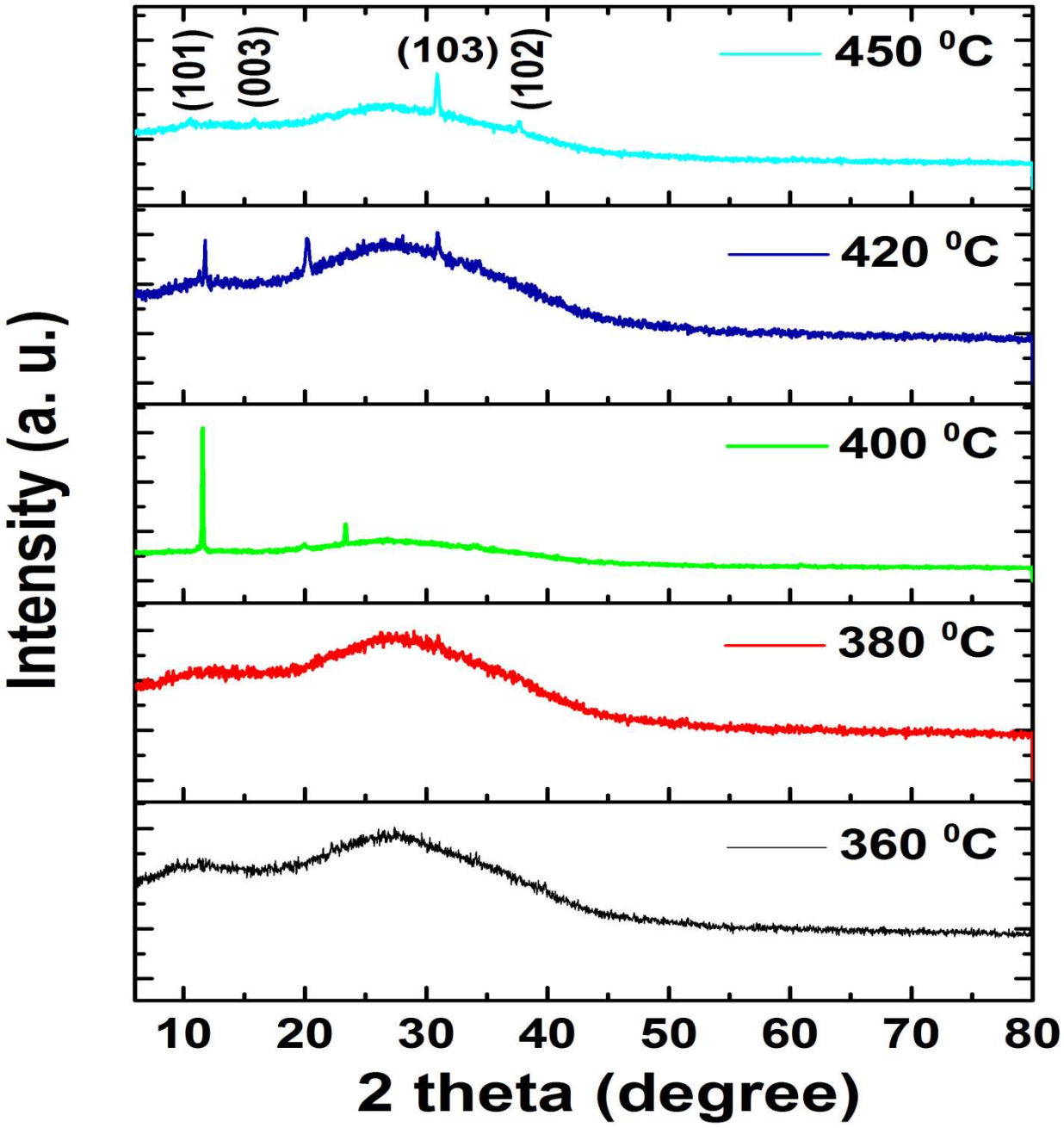

Figure 6: XRD pattern of the deposited Cu-Cd-S thin films

The average crystallite size of the as-deposited samples (see Table 3) was determined by the X-ray line broadening method via the Scherrer equation [32 , 33]:

$$L = \frac{k\lambda}{\beta Cos\theta} \qquad (1)$$

Where $\lambda = 0.1789\ nm$ is the wavelength of the radiation used, CoKα in this case, k is the Scherrer constant, β (radian) is the full width at half maximum (FWHM) intensity of the diffraction peak for which the size is to be determined, θ is the diffraction angle of the particular peak, and L is the crystallite size. The crystal size of the prepared film decrease as the deposition temperature increases. The internal strain and the broadening of the X-ray peaks are important influence on the crystal size.

From Bragg's equation [34], the Cu-Cd-S thin film XRD parameters were estimated for hexagonal structure (a = b ≠c) using the following equations and shown in Table 1.

$$\frac{1}{d^2} = \frac{4}{3}\left(\frac{h^2 + hk + k^2}{a^2}\right) + \frac{l^2}{c^2} \qquad (2)$$

$$Sin^2\theta = \left[\frac{\lambda^2}{4a^2}\left(\frac{4}{3}(h^2 + hk + k^2) + \frac{l^2}{\left(\frac{c}{a}\right)^2}\right)\right] \qquad (3)$$

where, d is interplanar spacing (nm), a and c are lattice parameters and hkl are miller indices. There were fluctuations in the value of lattice parameters at different temperatures, which indicated that temperature induced changes in electronic structure of the films has occurred [35].

Table 3: Estimated XRD parameters calculated for the deposited Cu-Cd-S thin films.

Temperature (°C)	θ°	FWHM	L (nm)	d (nm)	a (nm)	c (nm)
450	30.91	0.2809	35.56	0.1991	0.4010	0.6540
420	30.95	0.2158	46.30	0.0943	0.4326	0.7050
400	32.66	0.0497	201.58	0.1846	0.2052	0.3340
380	Amorphous					
360	Amorphous					

3.6 Morphology of Cu-Cd-S thin films

The micrographs of the deposited films at different deposition temperatures are shown in Figure 7 (a-e). Figure 7a shows the micrograph of film deposited at 360 °C, in which there appeared

to be agglomeration of grains. As the deposition temperature increased to 380 ºC (Figure 7b), the film appears to be dense, homogeneous with closely packed grains which covered the substrate surface well and more of granules were observed. At 400 ºC, as shown in the Figure 7c, smaller and tightly packed grains are noticed. These observed grains are evenly distributed across the substrate surface. At 420 ºC, as shown in Figure 7d, the film composed of smaller granules which are uniform and smooth on the substrate surface with a larger number of grains occupying smaller surface area of the film. This indicates an improvement in the crystallinity of the films as deposition temperature increases, which was also confirmed by the XRD pattern. Also, in Figure 7e at 450 ºC, it can be seen that the film has definite boundaries and the grains agglomerate to form a well-defined nanoplate and nanorod like structure. Similar result has been reported in the literature [30]. Generally, the films are uniform and crack-free which is the basic requirement for any device application. It can therefore be concluded that morphological properties of deposited films strongly depended on substrate temperature. This is in agreement with the work of Diwate *et al*., 2017 [36] who also reported similar result.

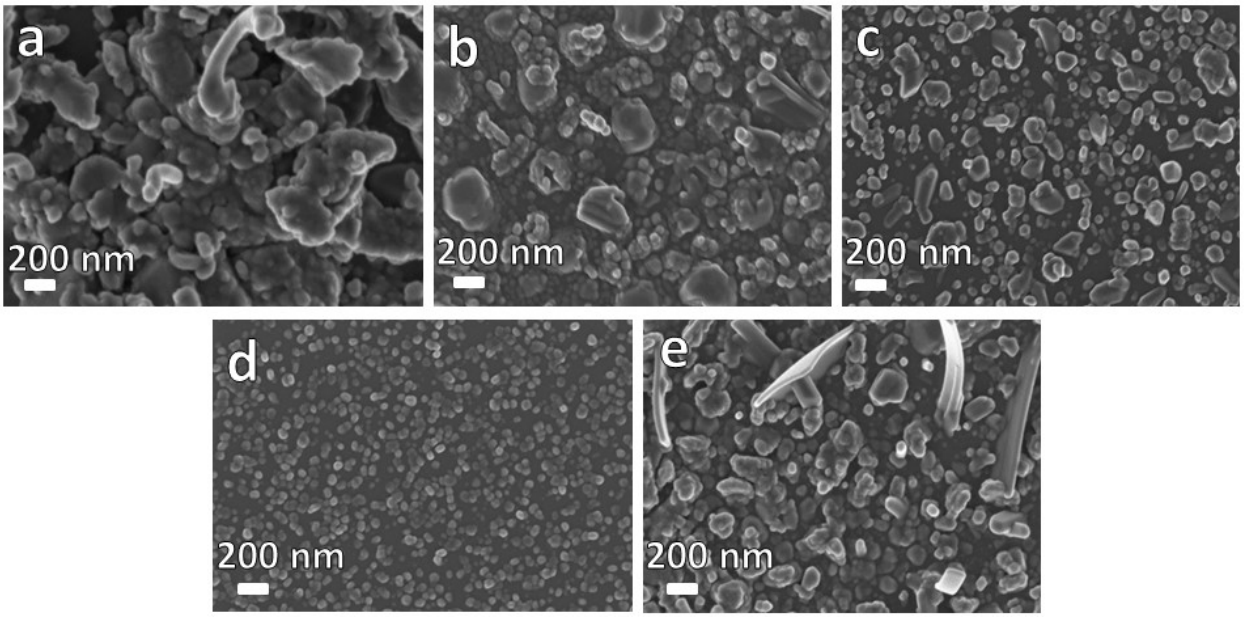

Figure 7: SEM micrograph of the deposited Cu-Cd-S thin films deposited at (a) 360 ^{o}C (b) 380 ^{o}C (c) 400 ^{o}C (d) 420 ^{o}C (e) 450 ^{o}C

3.7 Optical properties of the deposited Cu-Cd-S thin films

The study of optical properties of the deposited thin films was done using ultraviolet visible spectrophotometry. The plot of absorbance versus wavelength of the deposited Cu-Cd-S films is shown in Figure 8. All the absorbance spectra were acquired in the wavelength range 300 - 800 nm. As shown in the Figure, the absorbance of all the deposited films varies with wavelength in similar manner. Generally, all the films have high absorbance in the ultraviolet region after which they decreased rapidly within the visible region and almost constant near infrared region. The observed high absorbance in the ultraviolet region may be attributed to electronic inter-band transitions from the filled sulphide valence band through to the empty conduction band [37, 38]. It can also be as result of light scattering from the nanometer sized grains of the films as reported by Olofinjana *et al*., [39]. Also, it can be seen from Figure 8 that all the films have sharp absorption edge in the visible region. The observed sharp absorption edge indicates good quality films with low defect density near the band edge of the films [38]. The slight increase in absorption edge in the visible region when the deposition temperature increases may be due to increase in the degree of crystallization of the films. Therefore, increase in substrate temperature improves the absorbance of the films.

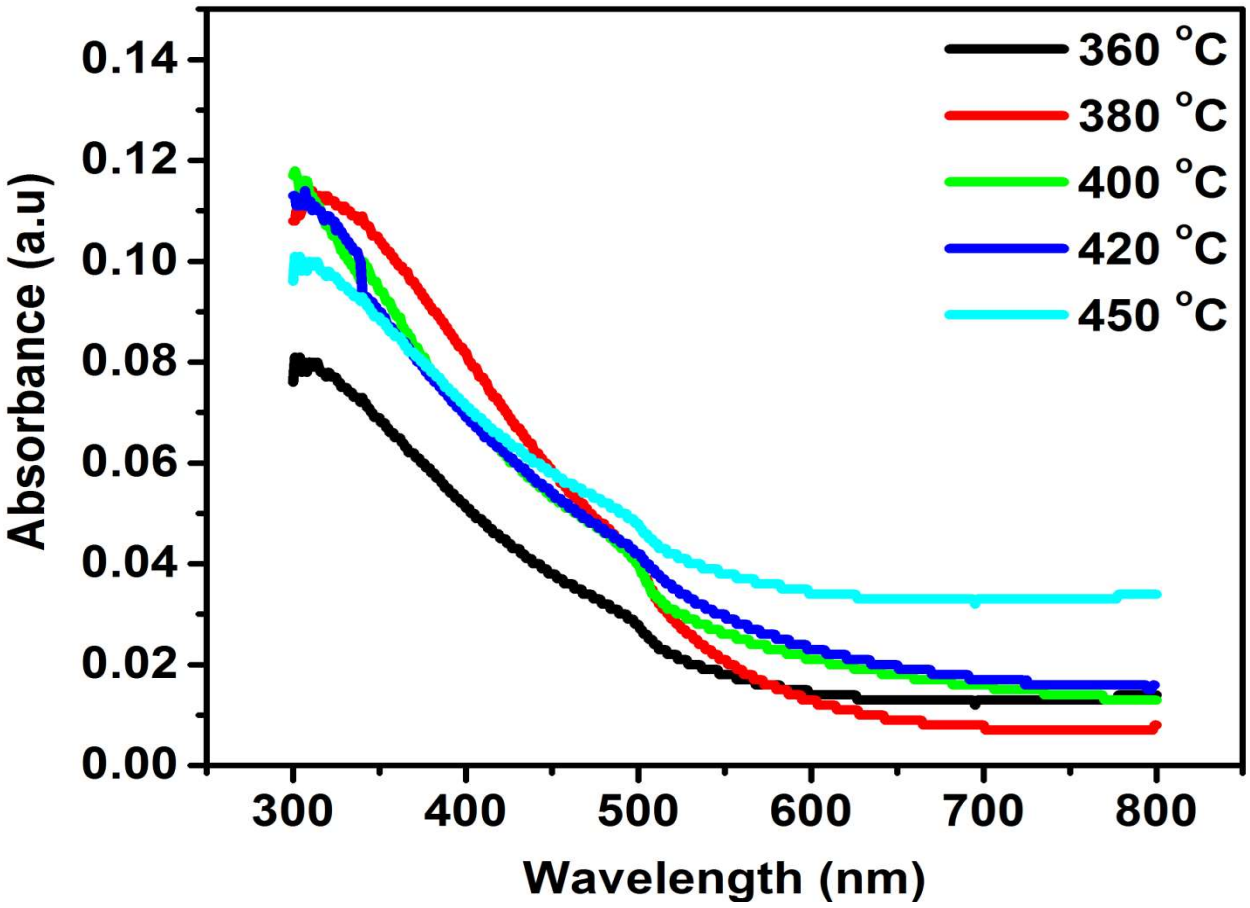

Figure 8: Absorbance against wavelength for the deposited Cu-Cd-S thin films

The transmittance of the deposited films was obtained using the relation:

$$T = 10^{-A} \qquad (4)$$

where T is the transmittance and A is the absorbance. The plot of transmittance against incident wavelength for the deposited Cu-Cd-S thin films at various deposition temperatures is shown in Figure 9. By increasing the substrate temperature in the range 360 ºC - 450 ºC, there was a sharp increase in transmittance from a value of about 89 % to about 97 % at 800 nm. This can be due to increase in crystallinity as the deposition temperature increases [38]. In addition, the spectra revealed that all the deposited thin films exhibit transmission above 75 % in the range 300 - 800 nm wavelength. High transmittance of the film indicated that the films can be used for several

applications, including solar cells, light emitting diodes and photonic devices and it can also be a good material for thermal control window coatings for cold climates and anti-reflection coatings.

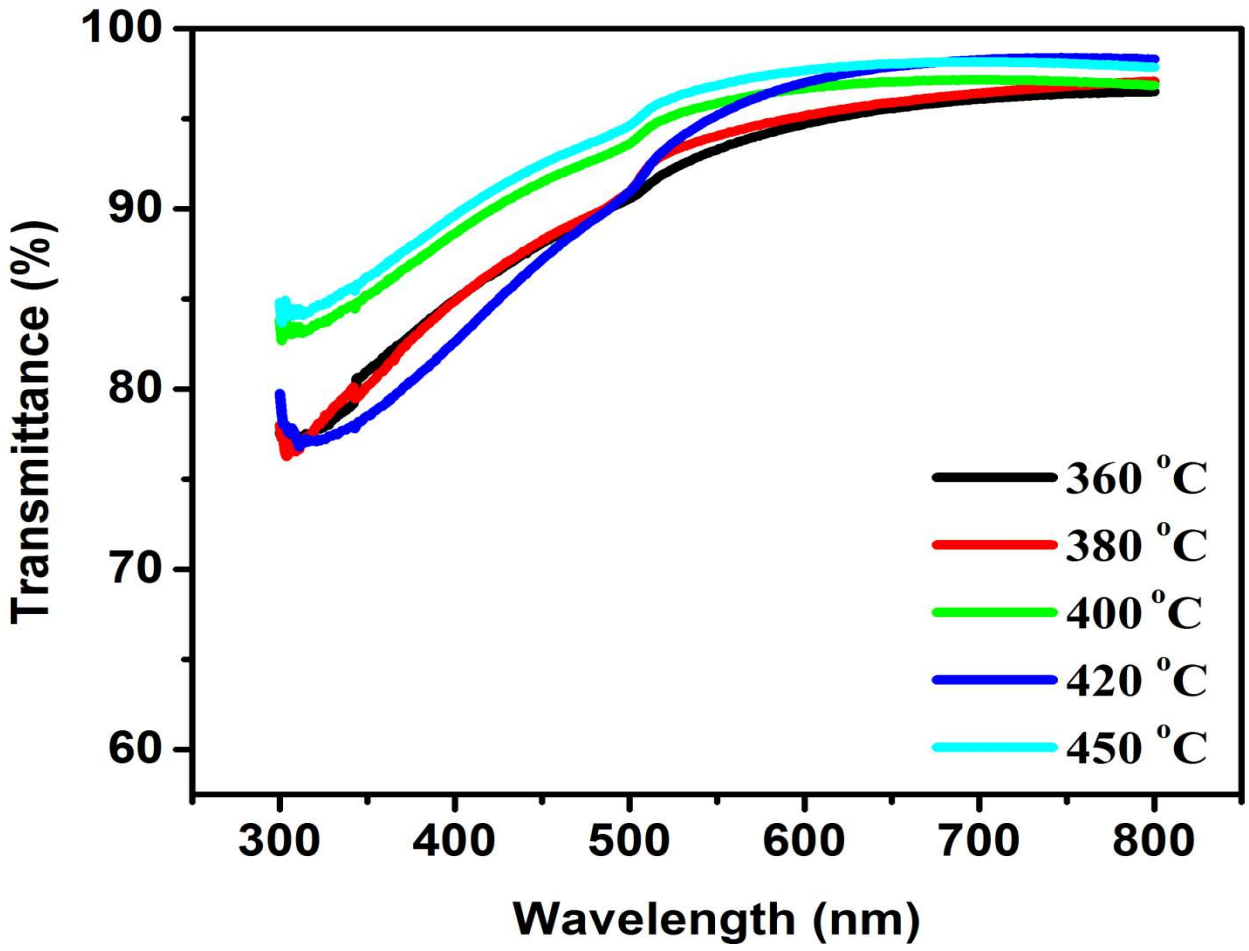

Figure 9: Transmittance against wavelength for the deposited Cu-Cd-S thin films

From the absorbance *A* and the film thickness, *t,* obtained from RBS result, the absorption coefficient, *α,* was calculated using equation [38,39].

$$\alpha = \frac{2.303A}{t} \qquad (5)$$

The energy was calculated in electron volts (eV) using the equation:

$$\mathrm{E} = \frac{\mathrm{hc}}{\lambda} \qquad (6)$$

where, h = Planck's constant, c = speed of light and λ = wavelength.

A graph of absorption coefficient *(α)* against photon energy was plotted in order to identify the type of transition present in the films. Figure 10 shows a graph of absorption coefficient against photon energy of the deposited films at various deposition temperatures. A single gradient was obtained from the plot, which indicates that direct transition is prevalent in the films.

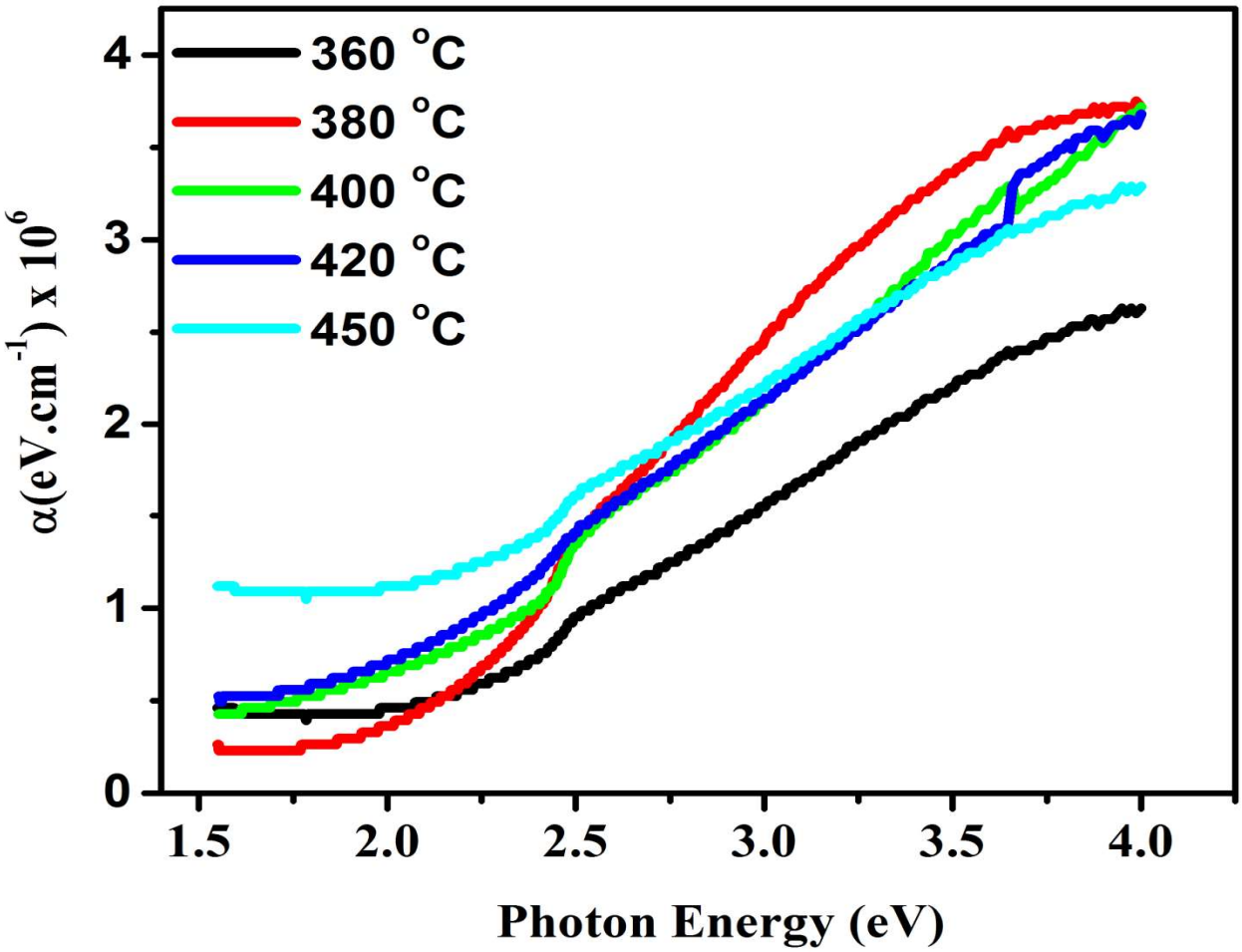

Figure 10: Absorption coefficient against photon energy for the deposited Cu-Cd-S thin films

The direct band gap energy E_g was calculated from the graph of α^2 against the photon energy (Figure 11). The value of E_g was evaluated by the extrapolation of the linear portion of the curve to $\alpha^2 = 0$ along the photon energy axis. The direct band gap of the deposited films varies from 2.36

to 2.14 eV (Table 4). Generally, in semiconducting materials, optical band gaps are mostly influenced by degree of crystallinity, crystallite size, defects, impurities and disorders of grain boundaries [40]. Decrease in E_g values with increase in deposition temperature can be explained in terms of increase in crystallinity, as it was observed in the XRD result. The Observed band gap can make the films to be a potential material for photovoltaic applications since maximum number of photons coming from solar radiation have wavelength in visible and near infrared regions.

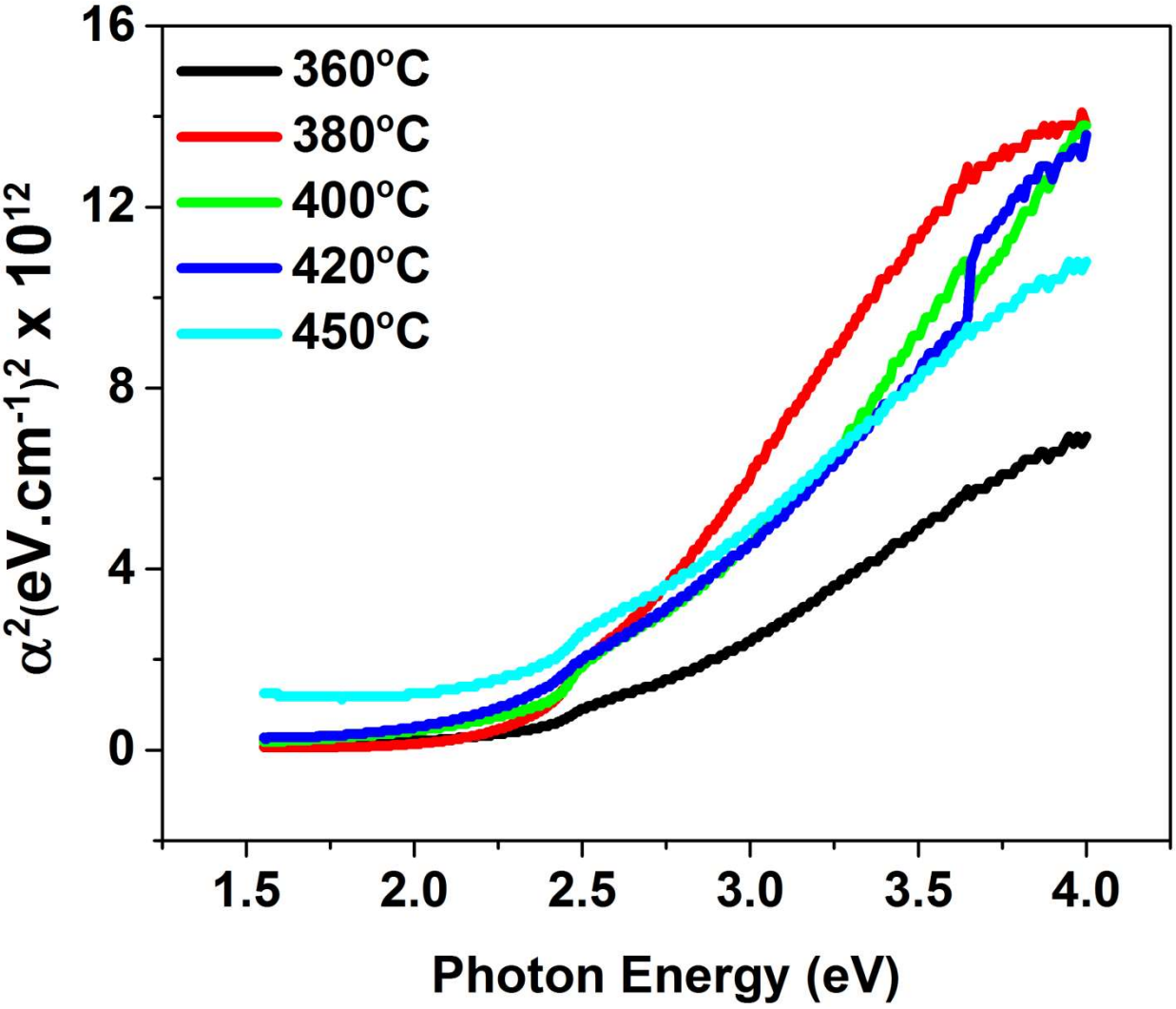

Figure 11: Square of absorption coefficient against photon energy for deposited Cu-Cd-S thin films

The Urbach energy is mostly used as a measure of the degree of structural disorder since the formation of localized states with energies at the boundaries of the energy gap is one of the effects of the structural disorder on the electronic structure of materials. The relationship between absorption coefficient (α) and photon energy (E) can be expressed as

$$\alpha = \alpha_o \exp\left(\frac{E}{E_u}\right) \quad (7)$$

where α_o is a temperature dependent constant and E_u is the Urbach energy.

Figure 12 shows the Urbach plot of $Ln\alpha$ against photon energy E for the deposited films at various deposition temperatures. The inverse of the gradient gave the Urbach energy. The Urbach energy of the deposited films increases from 0.72 to 1.34 eV (Table 4) as the deposition temperature increases. This increase in Urbach energy is associated with the increase of the localized states from non-radiative recombination centres [41, 42].

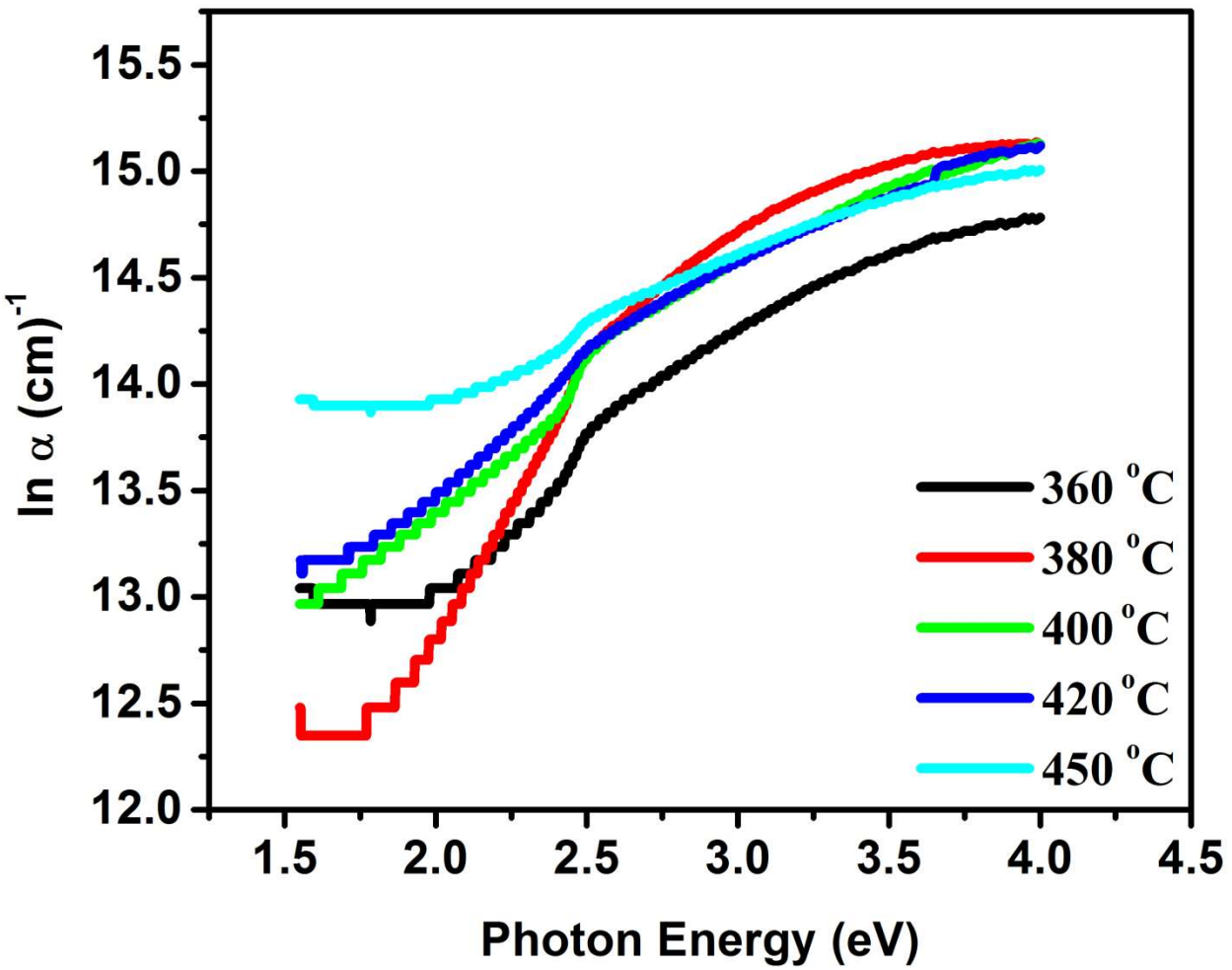

Figure 12: Plot of Lnα against photon energy

The steepness parameter, σ_{ste} which depict the broadening or shrinkage of the absorption edges caused by electron-phonon or exciton-phonon interactions can be computed using [41]

$$\sigma_{ste} = \frac{K_B T}{E_U} \qquad (8)$$

where K_B is the Boltzmann constant and T is absolute temperature in kelvin. The calculated σ_{ste} for all the deposited films at room temperature are listed in Table 4. σ_{ste} was noted to decrease from 0.033 to 0.018 as the deposition temperature increases. The decrease in σ_{ste} can be ascribed to increase in localized states which begin from the non-radiative recombination centers [40].

Table 4: Band gap, Urbach energy and steepness parameter of the deposited films

Deposition temperature ºC	Band gap (eV)	Urbach energy (eV)	Steepness parameter
360	2.36	0.72	0.033
380	2.32	0.86	0.027
400	2.28	1.12	0.021
420	2.26	1.13	0.020
450	2.14	1.34	0.018

One of the fundamental properties of an optical material is refractive index (n) since it is closely related to electronic polarization of ions and the field inside the materials. The refractive index of Cu-Cd-S thin films was obtained from the reflectance (R) of the films by using the relation in equation below [42]:

$$n = \frac{1+\sqrt{R}}{1-\sqrt{R}} \qquad (9)$$

From Figure 13, it was observed that refractive index at 360 ºC and 380 ºC decreases sharply as photon energy increases till about 2.5 eV, after which it decreases gradually, almost constant within 2.5 eV to 4.20 eV. It can also be seen that at 400 ºC, 420 ºC and 450 ºC refractive index increases steadily as photon energy increases till about 1.72 eV, after which it decreases sharply till about 2.5 eV and then decreases gradually, almost constant within 2.6 eV to 4.20 eV. At lower region of the photon energy, increase in refractive index can be due to an increase in surface roughness, which acts to decrease the effective mean free path by increasing the surface scattering. Also, the low refractive index at higher photon energy can be as a result of successive internal reflection or trapped phonon energy in the grain boundaries. Similar result has been reported in the literature [43].

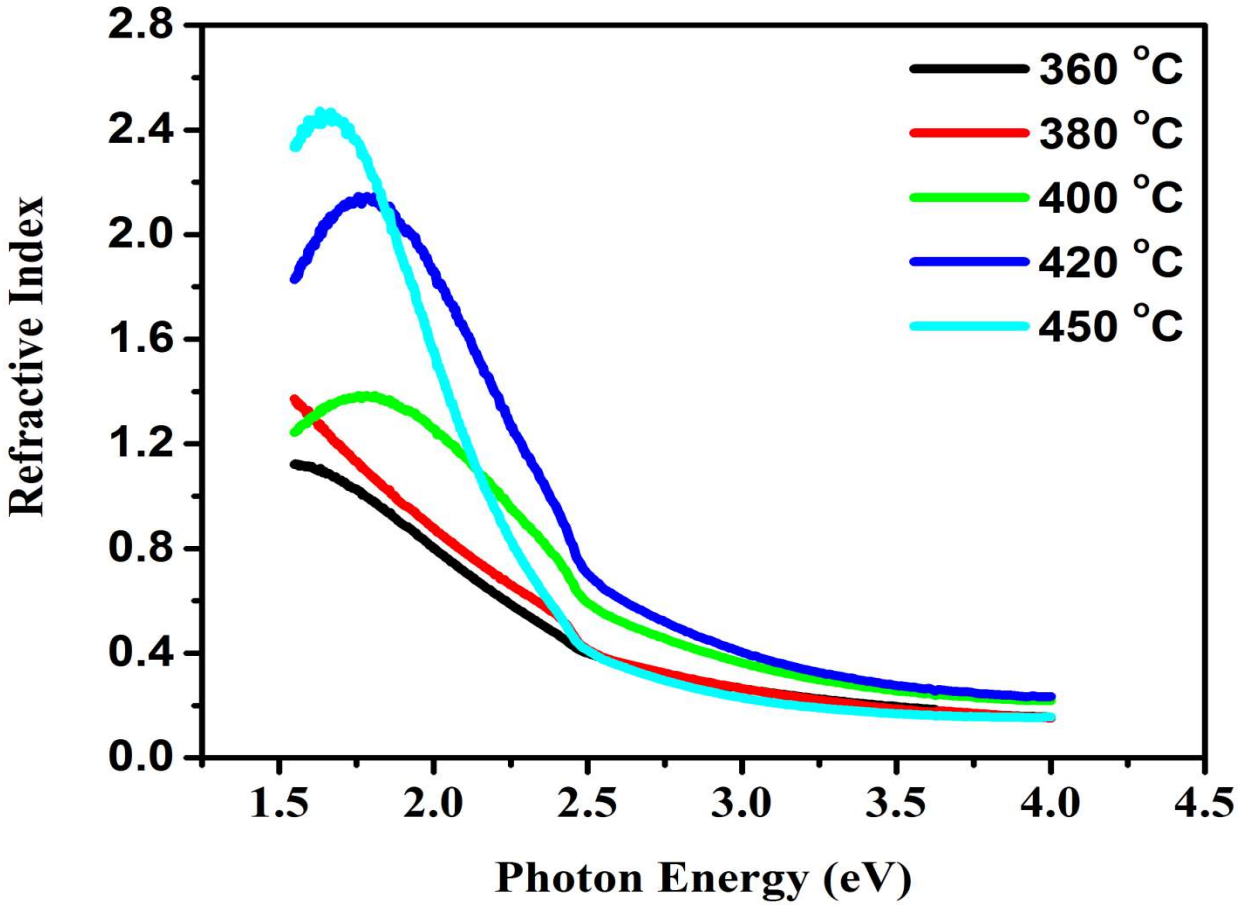

Figure 13: Plot of refractive index against photon energy for Cu-Cd-S thin films

Extinction coefficient is a measure of the amount of absorption loss when electromagnetic radiation propagates through the films. The extinction coefficient K was obtained using equation [42]:

$$K = \frac{\alpha \lambda}{4\pi} \qquad (10)$$

The graph of extinction coefficient K versus photon energy is shown in Figure 14. From the graph, it can be observed that the extinction coefficient of all the deposited films have the same pattern, in which it increases as photon energy increases. This can be as a result of successive internal reflection or due to trapped photon energy in the grain boundaries. In addition, it indicates that the

deposited films can be used for high-quality window materials so as to minimize absorption losses [44].

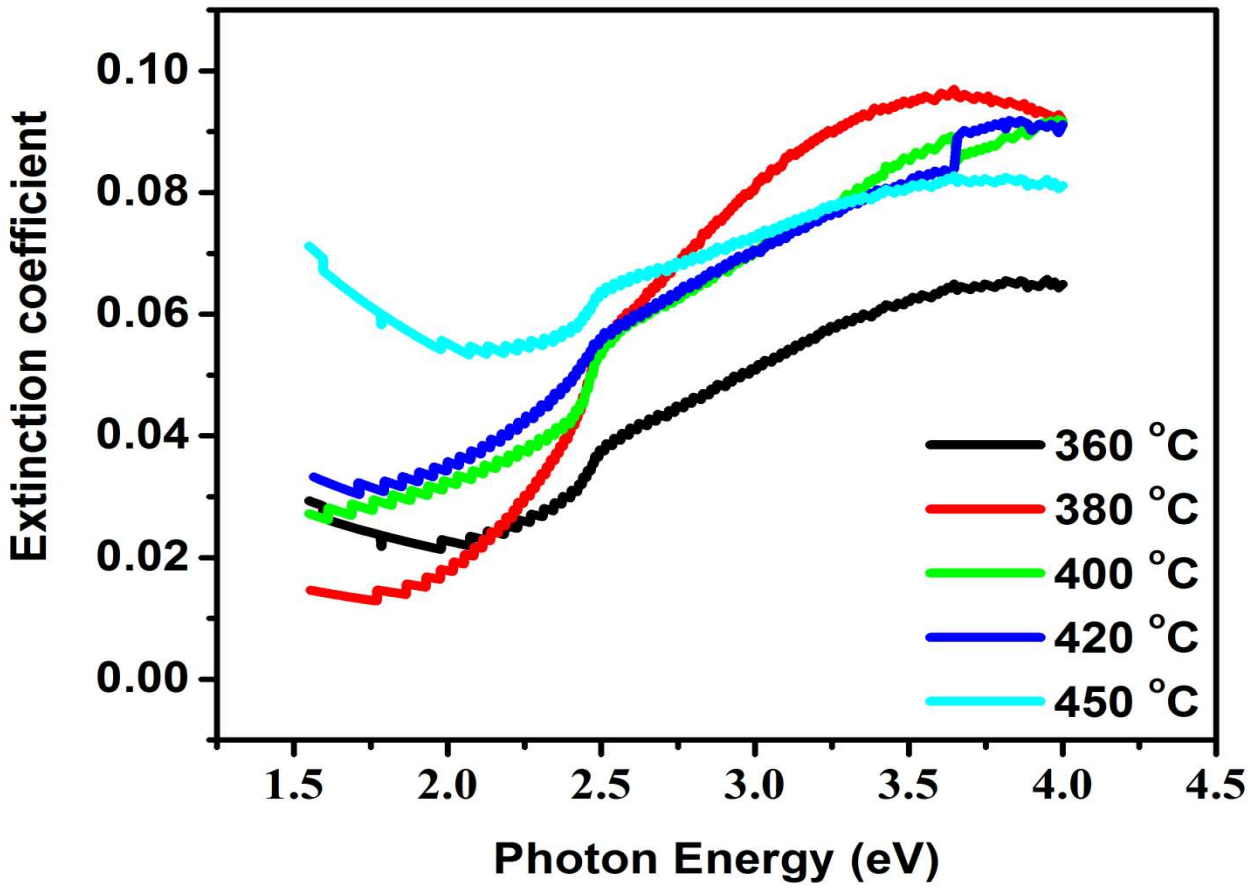

Figure 14: Extinction coefficient versus photon energy for Cu-Cd-S thin films

To investigate the electronic structure of the deposited films, it is necessary to consider dielectric properties of the deposited films. The real and imaginary parts of dielectric constant (ε_r and ε_i) of the deposited films can be evaluated by the following equations [42, 44]:

$$\varepsilon_r = n^2 - K^2 \quad (11)$$

$$\varepsilon_i = 2nK \quad (12)$$

The variation of the real dielectric constant (ε_r) and imaginary dielectric constant (ε_i) with photon energy for the deposited films at various deposition temperatures are shown in Figure 15 and Figure 16 respectively. From Figure 15, it was observed that the real part of dielectric constant for films deposited at 360 ºC and 380 ºC are similar. In both cases, ε_r decreases sharply as photon energy increases, to about 2.5 eV, after which it decreases gradually, almost constant within 2.5 to 4.20 eV. At 400 ºC, 420 ºC and 450 ºC the real part of dielectric constant initially increased at photon energy range of 1.55 - 1.77 eV, after which it decreases sharply till about 2.5 eV and then decreases slightly, almost constant within 2.5 to 4.20 eV. This behaviour was similar with that of refractive index due to the smaller value of extinction coefficient when compared to refractive index. In general, within the photon energy range of 1.5 to 2.5 eV, the real dielectric constant increases as substrate temperature increases. In the Figure 16, for the films deposited between 360 - 420 ºC, the imaginary part of dielectric constant decreases linearly in the photon energy range of 1.60 to 4.20 eV. At 450 ºC the imaginary part of dielectric constant decreases sharply from 0.26 - 0.09 as photon energy increases to about 2.5 eV, after which it decreases slightly within the photon energy range of 2.50 eV to 4.20 eV. The decrease in imaginary dielectric constant towards the higher photon energy might be due to light scattering from the nanometer sized grains of the films. It can also be as a result of minimal recombination losses and less interference on movement of charge carriers [45].

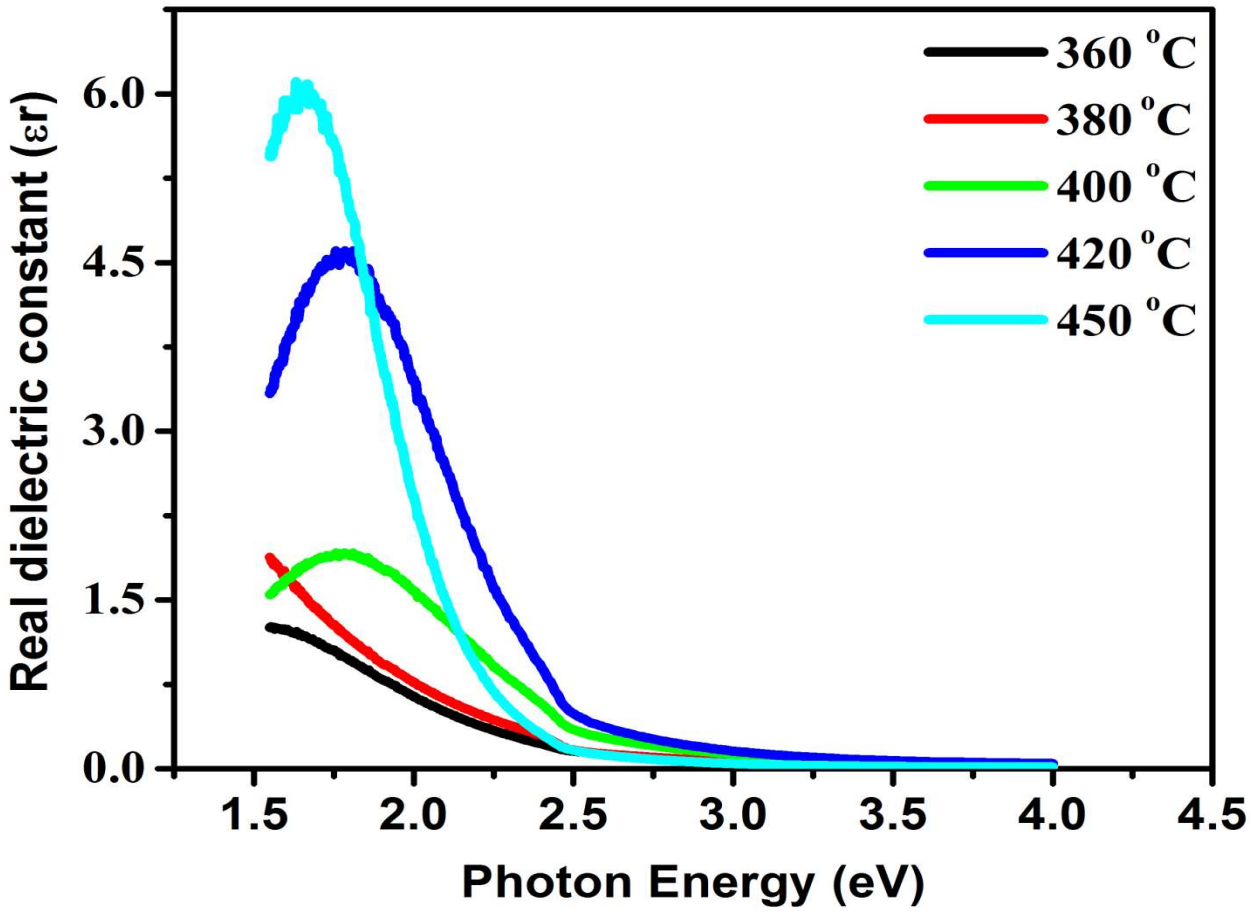

Figure 15: Real dielectric constant against photon energy

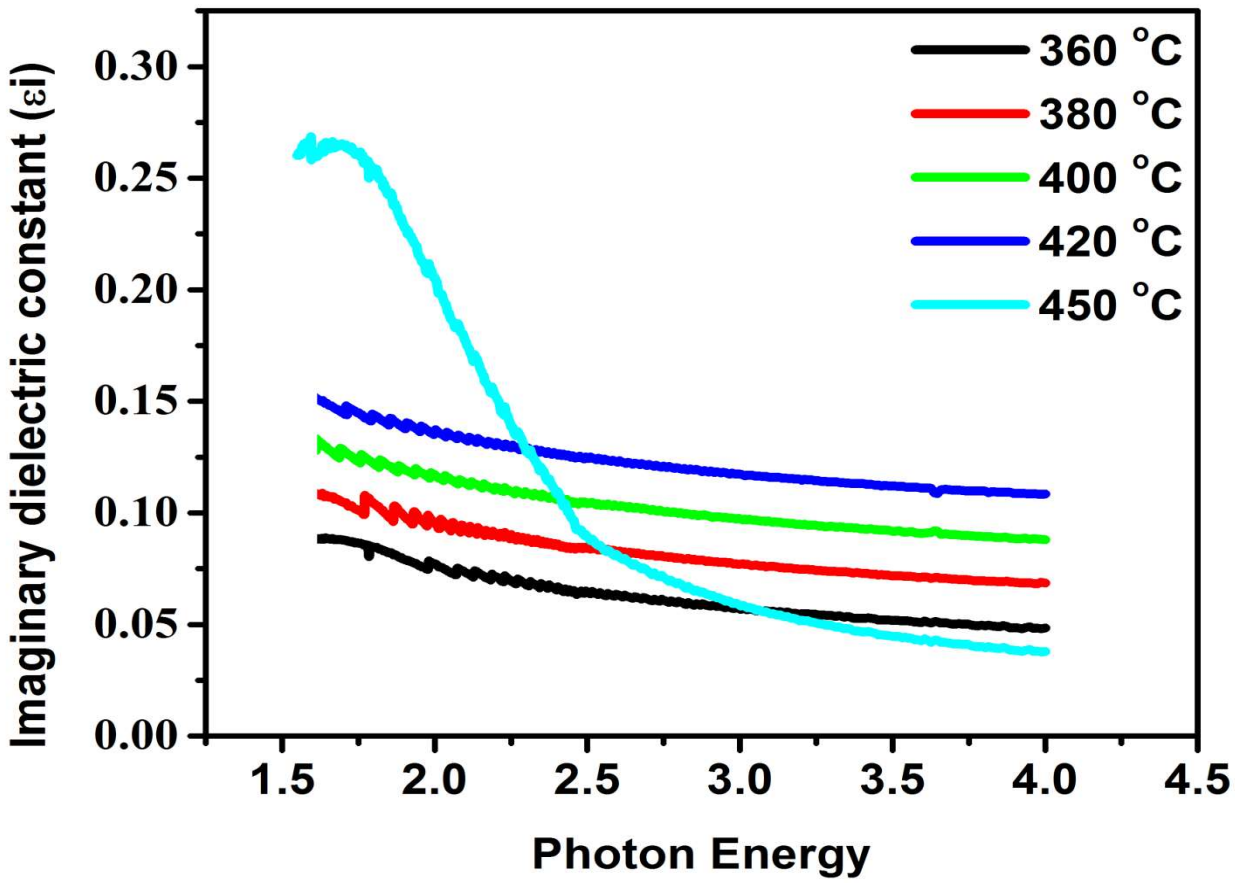

Figure 16: Imaginary dielectric constant against photon energy

The optical conductivity of the films was evaluated using the relation [44]

$$\sigma_{opt.} = \frac{\alpha n}{4\pi} \qquad (13)$$

where c is the speed of light. Figure 17 shows the plot of optical conductivity against photon energy of the deposited films. From the plot, it was observed that optical conductivity at 360 °C and 380 °C decreases sharply as photon energy increases till about 2.5 eV, after which it decreases gradually, almost constant within 2.5 to 4.20 eV. At 400, 420 and 450 °C optical conductivity increases initially in the photon energy range of 1.55 - 1.80 eV and then decreases sharply till about 2.5 eV, after which it then decreases gradually, almost constant within 2.5 to 4.2 eV. This behaviour can be attributed to high absorbance of the film in the ultraviolet region [44]. Generally,

it can be observed that the optical conductivity of the films increases as substrate temperature increases, which can be attributed to increase in the crystallinity as the deposition temperature increases.

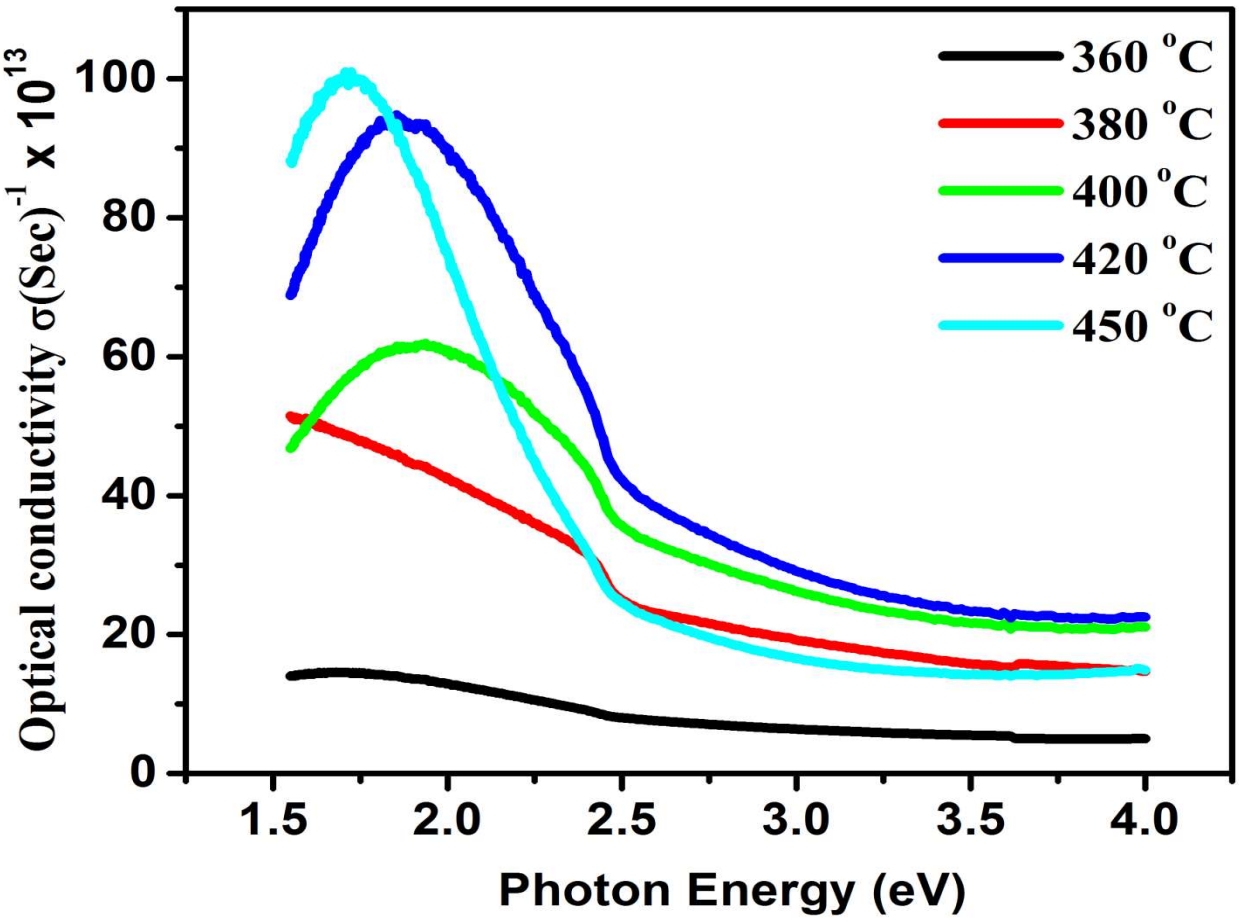

Figure 17: Optical conductivity against photon energy for the deposited Cu-Cd-S thin films

3.8 Electrical characterization of Cu-Cd-S thin films

The sheet resistance R_{sh} and resistivity ρ of the films were calculated from the expression in the following equations [28]:

$$R_{sh} = \frac{\rho}{t} = \frac{\pi}{\mathrm{In2}}\frac{\mathrm{V}}{\mathrm{I}} = 4.532\,\frac{\mathrm{V}}{\mathrm{I}} \quad (14)$$

$$\rho = \frac{\pi V}{ln(2)I}t \; = \; 4.532t\,\frac{\mathrm{V}}{\mathrm{I}} \quad (15)$$

where V is the voltage, I is the current and t is the thickness of the film. The results of sheet resistance, resistivity and conductivity of the deposited films are listed in Table 5. As it can be seen from Table 5, all films exhibited semiconductor behaviour with decrease in resistivity of deposited films from 18.12 x 10^{10} to 4.12 x 10^{10} $\Omega.cm$ as substrate temperature increases from 360 to 450 ^{o}C. This can be attributed to the increase in the crystallinity of the films as deposition temperature increases.

Figure 18 shows the graph of current I against voltage V of the deposited films at different deposition temperatures. From the plot, it can be observed that current increases linearly with the applied voltage which indicated that the films have ohmic characteristics. The resistance of the films was obtained by taking the inverse of the gradient of I-V plot in Figure 18. Decrease in resistance of the films was also reported in the literature [40] and it was attributed to the replacement of Cd^{2+} ions with Cu^{2+} ions in the lattice of CdS. This can also be true in this case. Also, it can be as a result of increase in the electrical conductivity and crystallinity of the films.

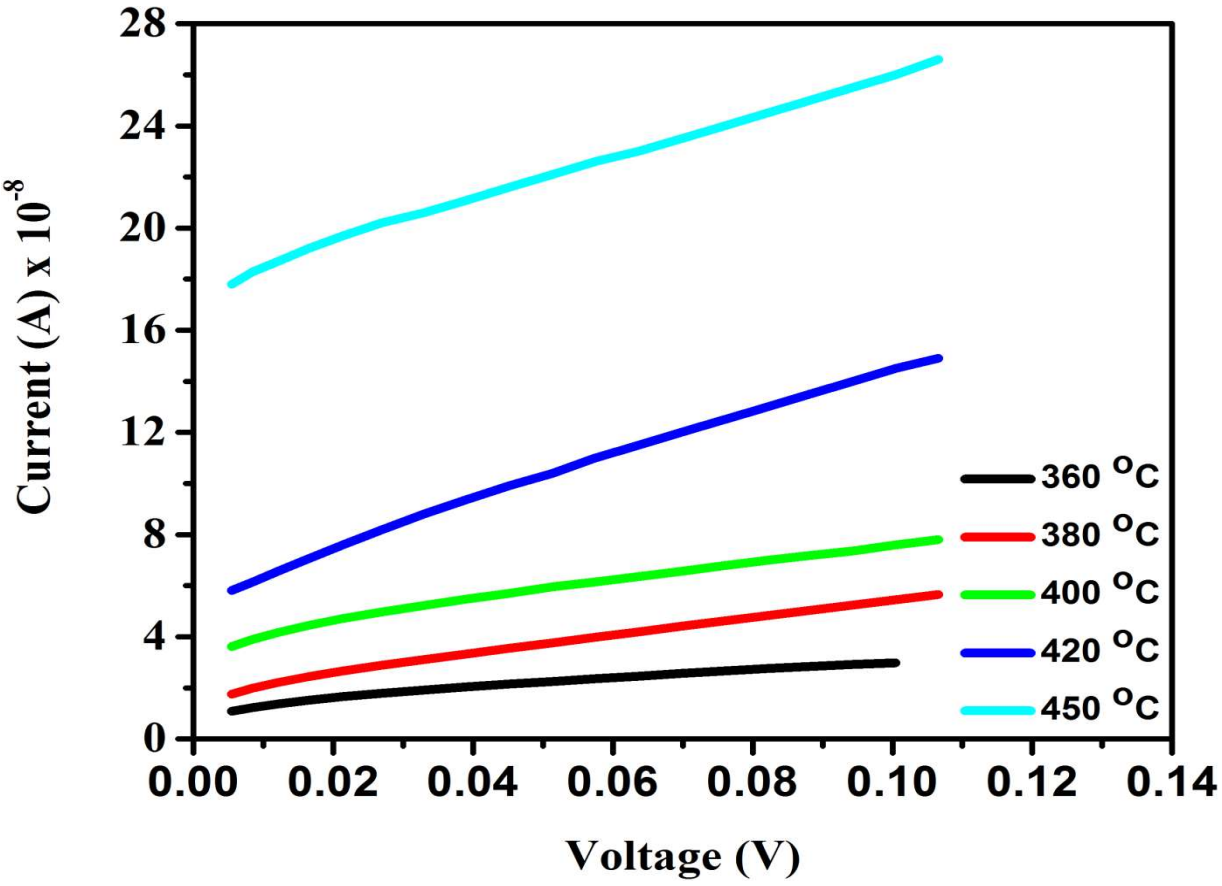

Figure 18: I-V characteristics of the deposited Cu-Cd-S thin films

Table 5: Values of sheet resistance, resistivity, conductivity and resistance of the Cu-Cd-S thin films at various deposition temperatures

Deposition temperature °C	Sheet Resistance (Ω/sq) x 10^8	Resistivity Ω.cm x 10^{10}	Conductivity $(Ω.cm)^{-1}$ x 10^{-11}	Resistance Ω x 10^6
360	45.32	18.12	0.55	10.00
380	22.66	11.33	0.88	5.00
400	13.59	8.15	1.22	3.33
420	7.25	4.71	2.12	1.67
450	5.89	4.12	2.42	1.25

4. Conclusion

A single solid source precursor, bis-(morpholinodithiato-s,s')-Cu-Cd was successfully synthesized by the reaction of different reagents. Characterization of the precursor was achieved using PIXE, FTIR and DTA. PIXE result revealed the presence of the expected elements - copper, cadmium and sulphur in the prepared precursor. FTIR revealed the presence of various characteristic bands of the organic ligands. DTA revealed that the synthesized precursor is thermally stable, which can pyrolyzed between 300 ^{o}C and 500 ^{o}C.

RBS of the films confirmed the presence of expected elements in various stoichiometry at different deposition temperature. This confirmed that the pyrolysis of bis-(morpholinodithiato-s,s')-Cu-Cd in nitrogen gas medium at various deposition temperatures produced Cu-Cd-S thin films of various stoichiometry, in which thickness was observed to increase from 40 to 70 nm as deposition temperature increased. Absence of impurity in the RBS result showed the quality of the MOCVD technique.

Observation from XRD pattern showed that the films deposited at 360 and 380 ^{o}C are amorphous in nature while those deposited at 400 to 450 ^{o}C showed peaks which supported the possible co-existence of CuS and CdS as Cu-Cd-S, with an improvement in the crystallinity as substrate temperature increases. The morphology of the films deposited at various deposition temperatures showed that the films are uniform and crack-free. The morphological properties of deposited films also strongly depended on substrate temperature.

The optical characterization showed that the films are highly absorbing in the ultraviolet region and highly transmitting in the visible and near infrared region of the electromagnetic spectrum. A decrease in energy gap from 2.36 to 2.14 eV was observed as deposition temperature increased. The Urbach energy increased from 0.72 to 1.34 eV while steepness parameter decreased

from 3.30 to 1.80 as the deposition temperature increased. The refractive index, extinction coefficient, optical conductivity, real and imaginary dielectric constants of the films increased as deposition temperature increased. Electrical characterization showed that for all the films deposited at various temperatures, the resistivity of the films reduced from 18.12 x 10^{10} to 4.12 x 10^{10} Ωcm while the resistance on the other hand, decreased from 10.00 x 10^{6} to 1.25 x 10^{6} Ω as deposition temperature increased. The decrease in resistivity with an increase in deposition temperature indicated semiconducting characteristics of the films.

References

[1] Pawar S M, Pawar B S, Kim J H, Joo O S and Lokhande C D 2011 Recent status of chemical of chemical bath deposited metal chalcogenide and metal oxide thin films *Curr. Appl. Phys.* **11** 117-161

[2] Su G, Hadjiev V G, Loya P E, Zhang J, Lei S, Maharjan S, Dong P, Ajayan P M, Lou J and Peng H 2015 Chemical vapor deposition of thin crystals of layered semiconductor SnS_2 for fast photodetection application *Nano Lett.* **15** 506-513

[3] Lee K, Gatensby R, McEnvoy N, Hallam T and Duesberg G S 2013 High performance sensors based on molybdenum disulphide thin films *Adv. Mater.* **25** 6699-6702

[4] Cao J, Wang Z, Zhan X, Wang Q, Safdar M, Wang Y and He J 2014 Vertical SnSe nanorod arrays: from controlled synthesis and growth mechanism to thermistor and photoresistor *Nanotech.* **25** 105705

[5] Zhang Y, Ye J, Matsuhashit Y and Iwasa Y, 2012 Ambipolar MoS_2 thin flake transistors *Nano Lett.* **12** 1136-1140

[6] Sutter-Fella, C M, Stuckalberger J A, Hagendorfer H, Mattina F L, Kranz L, Nishiwaki S, Uhl A R, Romanyuk Y E and Tiwari A N 2014 Sodium assisted sintering of chalcogenides and its

application to solution processed $Cu_2ZnSn(S,Se)_4$ thin film solar cells *Photovolt*. **26** 1420-1425

[7] Jackson P, Hariskos D, Lotter E, Paetel S, Wuerz R, Menner R, Wischmann W and Powalla M, 2011 New world record efficiency for Cu(In, Ga)Se_2 thin film solar cells beyond 20% *Photovolt*. **19** 894-897

[8] Kephart J M, Geistherdt R M and Sampath W S 2015 Optimization of CdTe thin film solar cell efficiency using a sputtered oxygenated CdS window layer *Photovolt*. **23** 1484-1492

[9] Obaid A S, Hassan Z, Mahdi M A and Bououdina M 2013 Fabrication and characterizations of n-CdS/p-PbS heterojunction solar cells using microwave assisted chemical bath deposition *Sol*. *Energy* **89** 143-151

[10] Meth J S, Zane S L, Sharp K G and Agrawal S 2003 Patterned thin film transistor incorporating chemical bath deposited cadmium sulphide as the active layer *Thin Solid Film* **444** 227-234

[11] Garcia L V, Loreda S L, Shaji S, Aguilar Martinez J A, Avellaneda D A, Das Roy T K and Krishnan B 2016 Structure and properties of CdS thin films prepared by pulsed laser assisted chemical bath deposition *Mater*. *Res. Bull.* **83** 459-467

[12] Zhang F, Wang S, Wang L, Lin Q, Shen H, Cao W, Yang C, Wang H, Yu L, Du Z, Xue J and Li L S 2016 Super colour purity green quantum dot light-emitting diodes fabricated by CdSe/CdS nanoplatelets *Nanoscale* **8** 12182-12188

[13] Wondmagegn W, Mejia I, Salas-Villasenor A, Stiegler H J, Quevedo-Lopez M A, Pieper R J and Gnade B E 2016 CdS thin film transistor for inverter and operational amplifier circuit applications *Microelectron. Eng.* **157** 64-70

[14] Tripathin S C and Jyoti R K, 2015 Investigation of non-linear optical properties of CdS/PS polymer nanocomposite synthesized by chemical route *Opt. Commun.* **352** 55-62

[15] Kalanur S S, Chae A Y and Joo O S 2013 Transparent $Cu_{1.8}S$ and CuS thin films on FTO as efficient counter electrode for quantum dot solar cells *Electrochem. Acta* **103** 91-95

[16] Patil A M, Lokhande A C, Chodankar N R, Shinde P A, Kim J H and Lokhande C D 2017 Interior design engineering of CuS architecture alteration with rise in reaction bath temperature for high performance symmetric flexible solid state supercapacitor *J Ind. Eng. Chem.* **46** 91-102

[17] Sabah F A, Ahmed N M, Hassan Z and Almessiere M A 2017 Influences of substrate type on the pH sensitivity of CuS thin films EGFET prepared by spray pyrolysis deposition *Mat. Sci. Semicon. Proc.* **63** 269-278

[18] Zhao L, Tao F, Quan Z, Zhou X, Yuan Y and Hu J 2012 Bubble template synthesis of copper sulphide hollow spheres and their applications in lithium ion battery *Mater. Lett.* **68** 28-31

[19] Nie G, Li Z, Lu X, Lei J, Zhang C and Wang C 2013 Fabrication of polyacrylonitrile/CuS composite nanofibers and their recycled applications in catalysis for dye degradation *Appl. Surf. Sci.* **284** 595-600

[20] Salavati-Niasari M, Hosseinpour S M, Mohandes F and Gholamrezaei S 2015 Characterization and photovoltaic studies of $CuInS_2$ nanostructures *J Mater. Sci. Mater. Electron.* **26** 2810-2819

[21] Kuamr V N, Suryakarthick R, Karuppusamy S, Gupta M, Hayakawa Y and Gopalakrishanan R 2015 Effect of precursor concentration on properties and tuning of conductivity between p-type and n-type $Cu_{1-x}Cd_xS_2$ thin films deposited by a single step solution process as a novel material for photovoltaic applications *RSC Adv.***5** 23015-23021

[22] Khan A H, Dalui A, Mukherjea S, Segre C U, Sarma D D and Acharya S 2015 Efficient solid-state light-emitting CuCdS nanocrystals synthesized in air *Angew. Chem.* **127** 2681-2686

[23] Cook W R, Shiozawa L and Augustine F 1970 Relationship of copper sulfide and cadmium sulfide phases *J Appl. Phys.* **41** 3058-3068

[24] Saravanan K, Suriakarthick R, Ananthakumar S, Babu S M and Selladurai S 2017 Colloidal synthesis of copper sulphide ($CuCdS_2$) nanoparticles and its structural, optical and morphological properties *Mater. Sci. Semicond. Proc.* **66** 123-130

[25] Reyes P and Velumani S 2012 Structural and optical characterization of mechanically synthesized copper doped CdS nanopowders *Mater. Sci. Eng. B* **177** 1452-1459

[26] Su J, Zhang T, Li Y, Chen Y and Liu M 2016 Photocatalytic activities of copper doped cadmium sulfide microspheres prepared by facile ultrasonic spray-pyrolysis method *Molecules* **21** 735-744

[27] Eleruja M A, Adedeji A V, Ojo I A O, Djebah A, Osasona O, Aladekomo J B and Ajayi E O B 1998 Optical characterization of pyrolytically deposited $Zn_xCd_{1-x}S$ thin films *Opt. Mater.* **10** 257-263

[28] Olofinjana B, Egharevba G O, Taleatu B A, Akinwunmi O O and Ajayi E O B 2014 Effect of deposition temperature on some properties of MOCVD molybdenum sulphide thin films *J Mater. Sci. Eng. B* **4** 78-85

[29] Kumar V N, Suriakarthick R, Hayakawa Y, Hussain S, Bhalerao G M, Gupta M, Sathe V and Gopalakrishnan R 2014 Deposition of $CuCdS_2$ thin film by single step solution process at low temperature as a novel absorber for photovoltaic applications *Superlattice Microst.* **76** 125-134

[30] Kashiwaba Y, Komatsu T, Nishikawa M, Ishiakaa Y and Segawa K 2002 X-ray diffraction studies of p-CdS:Cu thin films *Thin Solid Films* **408** 43-50

[31] Kumar N, Trilok K, Pathak L P, Purohit H C, Swarts Y C and Goswami C 2018 Self-assemble Cu doped CdS nanostructures on flexible cellulose acetate substrates using low cost sol-gel route *J Nano Struct. Nano Obj.* **16** 1-8

[32] Patra S, Mitra P and Pradhan S K 2011 Preparation of nanodimensional CdS by chemical dipping technique and their characterization *Mater. Res.* **14**, 17–20.

[33] Oyedotun K O, Madito M J, Momodu D Y, Mirghni A A, Masikhwa T M and Manyala N 2018 Synthesis of ternary NiCo-MnO_2 nanocomposite and its application as a novel high energy supercapattery device *J Chem. Eng.* **335** 416–433.

[34] Suryanarayana C and M Grant Norton 1998 *X-Ray Diffraction: A Practical Approach PlenumPress New York*

[35] Rao C N and Rao K K 1964 Effect of temperature on the lattice parameters of some silver–palladium alloys *Can. J Phys.* **42** 1336-1342

[36] Diwate K, Pawbake A, Rondiya S, Kulkami R, Waykar R, Jadhavar A, Rokade A, Funde A, Mohite K, Shinde M, Pathan H, Devan R and Jadkar S 2017 Substrate temperature dependent studies on properties of chemical spray pyrolysis deposited CdS thin films for solar cell applications *J Semicond.* **38** 023001

[37] Ramsarny K, Malik M A, Helliwell M, Raftery J and O'Brien P 2011 Thio-dithio-biuret precursors for zinc sulfide, cadmium sulfide and zinc cadmium sulfide thin films *Chem. Mater.* **23** 1471-1481

[38] Hossain M S, Kabir H, Rahman, M M, Hasan K, Bashar M S, Rahman M, Gafur M A, Islam S, Amri A, Jiang Z T, Altarawneh M and Dlugogorski B Z 2017 Understanding the shrinkage

of optical absorption edges of nanostructured Cd-Zn sulphide films for photothermal applications *Appl. Surf. Sci.* **392** 854-862

[39] Olofinjana B, Egharevba G O, Eleruja M A, Jeynes C, Adedeji A V, Akinwunmi O O, Taleatu B A, Mordi C U and Ajayi E O B 2010 Synthesis and some properties of metal organic chemical vapour deposited molybdenum oxysulphide thin film *J Mater. Sci. Technol.* **26** 552-557

[40] Mahesha M G, Maghana R N and Padivar M 2017 Investigation of annealing on thermally evaporated ZnSe thin films through spectroscopy techniques *Physica B* **520** 37-42

[41] Lim W F, Quah H J, Hassan Z, Radzali R, Zainal N and Yam F K 2015 Alteration of structural and optical properties in quartenary $Al_{0.1}In0_{.1}Ga_{0.8}N$ films using ultraviolet assisted photo-electrochemical etching route *J Alloys Compd.* **649** 337-347

[42] Kabir H, Rahman M M, Uddin K M and Bhuiyan A H 2017 Structural, morphological, compositional and optical studies of plasma polymerized 2-furaldehyde amorphous thin films *Appl. Surf. Sci.* **423** 983-994

[43] Uhuegbu C C, Babatunde E B and Oluwafemi C O 2008 The study of copper zinc sulphide ($CuZnS_2$) thin films *Turk. J Phys.* **32** 39-47

[44] Damisa J, Olofinjana B, Ebomwonyi O, Bakare F and Azi S O 2017 Morphological and optical studies of thin films of $CuAlS_2$ deposited by metal organic chemical vapour deposition technique *Mater. Res. Express* **4** 086412

[45] Ibrahim K, Rahman M M, Zhao X, Veder J P, Zhou Z, Mohammadpour E, Majeed R H, Nikoloski A N and Jiang Z T 2018 Annealing effects on microstructural, optical and mechanical properties of sputtered CrN thin film coatings: experimental studies and finite element modelling *J Alloys Compd.* **408** 451-464